RSC Advances

PAPER

View Article Online
View Journal | View Issue

Cite this: *RSC Adv.*, 2026, **16**, 19991

Enhanced nanoencapsulation of gentamicin, ciprofloxacin, and lysozyme in chitosan-MIL-53 metal–organic frameworks for a synergistic activity against drug-resistant *Salmonella* from poultry and human origins

Fatma Ibrahim Mohamed,[a] Mohamed Ali Ibrahim,[a] Gihan Kamal Abdel-Latef,[a] Mohamed M. Abdel-Rahim,[a] Salama A. S. Shany,[b] Rehab Mahmoud, *[cf] Samar M. Mahgoub,[d] Sarah I. Othman[e] and Sahar Abdel Aleem Abdel Aziz[a]

The escalating crisis of antimicrobial resistance (AMR), particularly in foodborne pathogens like non-typhoidal *Salmonella*, necessitates innovative therapeutic strategies. This study first characterized multidrug-resistant (MDR) *Salmonella* serovars isolated from poultry and clinical sources in Egypt, confirming high resistance rates to gentamicin and ciprofloxacin, mediated by **aadA*-2* and *qnrA* genes. To overcome this challenge, we engineered a novel, multi-agent nano-delivery system designed for synergy and controlled release. A Quality-by-Design (QbD) approach using a Box–Behnken design optimized the formulation of chitosan-based nanoparticles encapsulating gentamicin, ciprofloxacin, lysozyme, and MIL-53(Fe) metal–organic frameworks (MOFs). Molecular docking analysis supported the dual antibacterial and anti-virulence potential of the system, showing strong binding of its components to the *Salmonella* SipD invasion protein. The optimized hybrid nanoformulation exhibited favorable characteristics: a particle size of 248 ± 11 nm, a positive zeta potential (+33.8 mV), and efficient encapsulation of all agents. It demonstrated superior *in vitro* antibacterial efficacy against MDR *Salmonella* isolates, evidenced by the largest inhibition zone (19.33 ± 1.76 mm), the lowest minimum inhibitory concentration (MIC) (2.93 ± 0.73 μg mL^{-1}) and minimum bactericidal concentration (MBC) (4.40 ± 2.20 μg mL^{-1}) values, and a fractional inhibitory concentration index (FICI) of 0.15, confirming strong synergy. Crucially, the formulation provided sustained release over 72 hours, fitting the Higuchi diffusion model, in stark contrast to the rapid release of free drugs. The novelty of this work lies in the rational design and statistical optimization of a chitosan-MOF hybrid system for the synergistic co-delivery of two antibiotics with a membrane-disrupting enzyme, creating a potent, sustained-release weapon against MDR *Salmonella*. This platform promises enhanced therapeutic efficacy, reduced dosing frequency, and a potential decrease in resistance development.

Received 26th December 2025
Accepted 2nd April 2026

DOI: 10.1039/d5ra09975g

rsc.li/rsc-advances

1 Introduction

The growing global demand for animal protein has led to an intensified use of antimicrobials in poultry production for therapy, prophylaxis, and growth promotion.[1] This practice exerts profound selective pressure, driving the emergence and dissemination of antimicrobial-resistant (AMR) bacteria, such as non-typhoidal *Salmonella*. These pathogens pose a dual threat: causing significant economic losses in poultry with mortality rates up to 80% in chicks and acting as a major source of foodborne zoonotic infections in humans, resulting in millions of cases of gastroenteritis annually.[2,3] Treatment of severe infections relies on antibiotics like fluoroquinolones (*e.g.*, ciprofloxacin) and aminoglycosides (*e.g.*, gentamicin). However, rising resistance to these critical drugs, compounded

[a]*Department of Hygiene, Zoonoses and Epidemiology, Faculty of Veterinary Medicine, Beni-Suef University, Beni-Suef, Egypt. E-mail: Mohamed1400@hotmail.com; gehankamal2008@outlook.com; m.abdelrahim@vet.bsu.edu.eg; fibhrahem1995@gmail.com; abdelaziz.sahar@yahoo.com*

[b]*Department of Poultry Diseases, Faculty of Veterinary Medicine, Beni-Suef University, Beni-Suef 62511, Egypt. E-mail: salama.shany@vet.bsu.edu.eg*

[c]*Department of Chemistry, Faculty of Science, Beni-Suef University, Beni-Suef 62511, Egypt. E-mail: rehabkhaled@science.bsu.edu.eg*

[d]*Department of Materials Science and Nanotechnology, Faculty of Postgraduate Studies for Advanced Sciences, Beni-Suef University, Beni-Suef, Egypt. E-mail: miramar15@yahoo.com*

[e]*Department of Biology, College of Science, Princess Nourah bint Abdulrahman University, P.O. Box 84428, Riyadh 11671, Saudi Arabia. E-mail: sialothman@pnu.edu.sa*

[f]*Department of Chemistry, Faculty of Science, Chulalongkorn University, Bangkok 10330, Thailand*

by their inherent limitations such as the poor intracellular penetration of gentamicin and the solubility issues and systemic toxicities (*e.g.*, nephrotoxicity, neurotoxicity) associated with both classes, has created a therapeutic impasse.[4,5]

The choice of antimicrobial agents in this study was driven by their clinical relevance and complementary mechanisms of action. Gentamicin, an aminoglycoside antibiotic, was selected because it is a first-line treatment for severe *Salmonella* infections; however, its clinical utility is increasingly compromised by widespread resistance mediated by aminoglycoside-modifying enzymes such as AadA-2, as well as its poor ability to penetrate intracellular compartments where *Salmonella* resides.[6] Ciprofloxacin, a fluoroquinolone, was chosen due to its potent bactericidal activity against Gram-negative pathogens through inhibition of DNA gyrase and topoisomerase IV. Nevertheless, plasmid-mediated quinolone resistance genes such as *qnrA* have significantly reduced their efficacy, and their use is associated with dose-dependent toxicity concerns.[7] The combination of gentamicin and ciprofloxacin was selected based on evidence that these two antibiotic classes exhibit synergistic activity when used together, as they target different bacterial processes, including protein synthesis and DNA replication, respectively, thereby reducing the likelihood of resistance development.[8]

Lysozyme, a naturally occurring bacteriolytic enzyme, was incorporated into the formulation for its ability to hydrolyze glycosidic bonds in peptidoglycan, the structural polymer of bacterial cell walls.[9] While Gram-negative bacteria like *Salmonella* are protected by an outer membrane that limits lysozyme access, we hypothesized that combining lysozyme with membrane-disrupting agents would expose the underlying peptidoglycan layer, enabling enzymatic degradation and enhancing bacterial killing.[9] This "priming" strategy is central to our multi-mechanistic approach. Recent studies have demonstrated that engineering enzymes to penetrate the outer membrane can render them highly bactericidal against Gram-negative pathogens, supporting the rationale for combining lysozyme with membrane-disrupting agents.[10]

Nanoencapsulation presents a promising strategy to revitalize existing antibiotics. By entrapping drugs within nanocarriers, their pharmacokinetics can be optimized: enhancing bioavailability, facilitating targeted delivery, enabling sustained release to maintain effective concentrations, and reducing off-target toxicity.[6] The choice of chitosan as the primary polymeric matrix was based on its well-documented biocompatibility, biodegradability, and mucoadhesive properties. Chitosan is a cationic polysaccharide derived from chitin, and its positive charge enables electrostatic interaction with negatively charged bacterial membranes, contributing to its intrinsic antibacterial activity.[7] Recent advances in chitosan nanoparticle synthesis have demonstrated their efficacy as drug delivery vehicles, with the ability to self-assemble into stable nanostructures that enhance antimicrobial activity through membrane perturbation mechanisms.[11,12]

Furthermore, chitosan can be cross-linked with sodium tripolyphosphate (TPP) *via* ionic gelation to form stable nanoparticles under mild conditions, making it an ideal carrier for sensitive biomolecules like lysozyme.[7] Studies have shown that quaternized chitosan derivatives exhibit enhanced stability in enzyme-rich environments and effectively inhibit multidrug-resistant bacteria through membrane disruption while preventing resistance development.[13,14]

Metal–Organic Frameworks (MOFs) are a class of hybrid materials composed of metal ions coordinated to organic linkers, forming highly porous structures with enormous surface areas. MIL-53(Fe), an iron-based MOF with terephthalic acid as the organic linker, was specifically selected for several reasons. First, its large pore volume and high surface area make it exceptionally suitable for high-capacity drug loading, particularly for aromatic drugs like ciprofloxacin that can interact *via* π–π stacking with the benzene rings of the linker.[15] Recent investigations of MIL-53(Fe) as an antibiotic-releasing material have demonstrated its ability to adsorb and release penicillin G through diffusion-controlled mechanisms, with the adsorption involving multiple types of interactions between the drug and the MOF framework.[16] Second, iron is a biocompatible metal that is endogenously regulated in biological systems, reducing toxicity concerns. Iron-based MOFs have shown blood compatibility and can be eliminated through urine and feces, making them suitable for biomedical applications.[17] Third, the gradual release of Fe^{3+} ions from the MOF framework under physiological conditions may contribute additional antibacterial effects by generating reactive oxygen species (ROS) and disrupting bacterial membrane potential.[18] Fourth, MIL-53(Fe) has demonstrated good stability and controlled release properties in previous biomedical applications.[19] The structural flexibility, high surface area, and abundant active sites of MIL-53 make it particularly effective for drug delivery applications, with the multidimensional network structure allowing adsorption of diverse organic molecules.[20]

The rationale for combining all these components into a single hybrid nanosystem is rooted in the concept of multi-mechanistic synergy. We hypothesized that the cationic chitosan would electrostatically interact with the negatively charged lipopolysaccharide (LPS) layer of the *Salmonella* outer membrane, increasing its permeability. Concurrently, Fe^{3+} ions released from the MIL-53(Fe) framework would further destabilize membrane integrity. This combined membrane-priming effect would then facilitate two critical events: (i) enhanced penetration of lysozyme to reach and degrade the peptidoglycan layer, and (ii) improved intracellular accumulation of gentamicin and ciprofloxacin, overcoming the poor penetration that limits their efficacy against intracellular pathogens. Recent research has demonstrated that the peptidoglycan layer forms a mechanical unit with the outer membrane, and disrupting this unit through membrane permeabilization can render Gram-negative bacteria susceptible to lysis.[21,22] Once inside the bacterial cell, the two antibiotics would exert their complementary bactericidal effects on protein synthesis and DNA replication, respectively. Furthermore, the porous structure of MIL-53(Fe) provides an ideal reservoir for ciprofloxacin, enabling sustained release, while the chitosan matrix entraps the water-soluble gentamicin and lysozyme, allowing for controlled delivery of all three agents from a single platform.

Studies of antibiotic-loaded nanoparticles have shown that effective MIC50 values can be decreased by more than 50% through nanoformulation, with synergistic combinations further enhancing potency.[23,24]

This integrated approach offers several potential advantages over conventional therapy: (i) synergistic enhancement of antibacterial activity through simultaneous action on multiple bacterial targets; (ii) overcoming existing resistance mechanisms by combining agents with different modes of action and by using physical membrane disruption that is not susceptible to enzymatic inactivation; (iii) sustained release that maintains therapeutic drug concentrations at the infection site while reducing systemic toxicity; and (iv) potential anti-virulence effects through interference with the Type III secretion system, as suggested by our molecular docking studies.

Therefore, this study had two primary objectives: first, to characterize the phenotypic and genotypic AMR profiles of *Salmonella* isolates from poultry and clinical settings in Beni-Suef, Egypt. Second, to develop, optimize, and comprehensively evaluate a novel nanoformulation co-encapsulating gentamicin, ciprofloxacin, and lysozyme within a chitosan-MIL-53(Fe) hybrid matrix for synergistic and sustained action against these MDR pathogens. Building upon our group's previous work, which established the prevalence of MDR *Salmonella* in poultry environments and the proof-of-concept that bare metal–organic frameworks (MOFs) possess intrinsic antibacterial activity, the current study represents a substantial and multi-faceted advancement. Here, we move beyond the use of simple MOFs as direct agents to introduce a rationally designed, hybrid nano-delivery platform. This sophisticated system leverages a MIL-53(Fe) MOF not as the primary killer, but as a high-capacity, porous carrier within a chitosan matrix, engineered for the synergistic co-delivery of two antibiotics and a bacteriolytic enzyme. Unlike our previous work, this study employs a Quality-by-Design (QbD) approach for statistical optimization, delves into the powerful synergistic interactions (FICI) between the five components, provides detailed kinetic modeling of sustained drug release, and offers a molecular rationale for the enhanced efficacy through computational docking against a key bacterial virulence protein (SipD). This multi-mechanistic strategy, combining potent bactericidal action with a potential anti-virulence effect, represents a significant leap forward in the development of advanced therapeutic platforms to combat the growing threat of MDR *Salmonella*.

2 Materials and reagents

2.1. Chemicals, reagents, and biologicals

Gentamicin sulfate (of potency ≥590 μg gentamicin per mg), ciprofloxacin hydrochloride (of purity 98.78%), and lysozyme from chicken egg white (of enzymatic activity ≥40 000 units per mg) were procured from Sigma-Aldrich (St. Louis, MO, USA). Low molecular weight chitosan (190 kDa, 75–85% deacetylated), sodium tripolyphosphate (TPP, 85%), iron(III) chloride hexahydrate ($FeCl_3 \cdot 6H_2O$, 97%), terephthalic acid (H_2BDC, 98%), (DMF, 99.8%), glacial acetic acid (≥99.7%), dimethyl sulfoxide (DMSO, ≥99.9%), and absolute ethanol were purchased from Sigma-Aldrich (St. Louis, MO, USA). Ampicillin (AMP, 10 μg), amoxicillin–clavulanate (AMC, 30 μg), cefoxitin (CX, 30 μg), ceftriaxone (CRO, 30 μg), nalidixic acid (NA, 30 μg), ofloxacin (OFX, 5 μg), enrofloxacin (5 μg), amikacin (AK, 30 μg), co-trimoxazole (COT, 25 μg), doxycycline (DO, 30 μg), clindamycin (DA, 2 μg), erythromycin (ERY, 15 μg), and fosfomycin (FO, 200 μg) were obtained from Oxoid (Basingstoke, UK). Standard antibiotic discs were purchased from HiMedia Laboratories (Mumbai, India).

Nutrient Agar (NA), Mueller–Hinton Agar (MHA), Mueller–Hinton Broth (MHB), Tryptone Soya Broth (TSB), and Brain Heart Infusion (BHI) broth and agar were all of microbiological grade and purchased from Oxoid Ltd (Basingstoke, Hampshire, United Kingdom).

The QIAamp DNA Mini Kit for genomic DNA extraction was obtained from Qiagen (Hilden, Germany). EmeraldAmp® Max PCR Master Mix (2× Premix) was purchased from Takara Bio Inc. (Shiga, Japan). Custom oligonucleotide primers for **aadA-2** and *qnrA* genes were synthesized by Metabion International AG (Planegg, Germany). Agarose, ethidium bromide, and 100 bp DNA ladder were sourced from Applied Chem GmbH (Darmstadt, Germany).

Sodium chloride, disodium hydrogen phosphate, and sodium dihydrogen phosphate were of analytical grade from El-Nasr Pharmaceutical Chemicals Co. (Cairo, Egypt). All aqueous solutions were prepared using deionized water (resistivity 18.2 MΩ cm) from a Milli-Q® purification system (Merck Millipore). Cellulose dialysis tubing (MWCO 12–14 kDa) was from Spectrum Labs (Rancho Dominguez, CA, USA).

2.2. Bacterial isolates and sample collection

A total of thirteen (13) confirmed *Salmonella* isolates were utilized in this study. The isolates comprised a panel of epidemiologically relevant serovars: *Salmonella typhimurium* ($n = 2$), *Salmonella enteritidis* ($n = 1$), *Salmonella infantis* ($n = 1$), *Salmonella virchow* ($n = 2$), *Salmonella kentucky* ($n = 2$), *Salmonella peniscola* ($n = 1$), *Salmonella grampian* ($n = 1$), and *Salmonella gueuletapee* ($n = 1$). Eleven (11) isolates were recovered from broiler chickens (*Gallus domesticus*). Samples were collected from birds aged 3–5 weeks, presenting clinical signs indicative of salmonellosis, including diarrhea, anorexia, dehydration, and pasty vents. The chickens were sourced from random broiler farms employing a deep-litter rearing system across different localities in the Beni-Suef province, Egypt, between January and October 2024. Post-mortem examinations were conducted under aseptic conditions, and samples from internal organs specifically the gall bladder, liver, bone marrow, and intestine were collected for bacteriological analysis. Further, two (2) additional isolates (*S. typhimurium*, and *S. enteritidis*) were obtained from stool samples of inpatients diagnosed with gastroenteritis at the Internal Medicine Department of Beni-Suef University Hospital, Beni-Suef governorate, Egypt. These isolates were included to assess the potential zoonotic link and cross-resistance patterns.

All specimens were processed in accordance with standard sanitary guidelines where, the chicken samples collected in the current study were officially approved by International Animal

Care and Use Committee (IACUC) of Beni-Suef University with reference number of 022-467. Also, after the sample collection by slaughtering, the humane endpoints criteria included in the ethical approval instructions were followed to prevent unnecessary suffering, and the samples were hygienically disposed. For the human sampling (stool), informed consents from the screened inpatients were obtained, and the samples were gathered in the rules and guidelines of Institutional Review Board (IRB) of Beni-Suef University with reference number of 022-467. Further, both type of samples, poultry and human ones, were immediately transported to the laboratory and processed for the bacteriological schemes.

Salmonella isolation and biochemical identification were performed using established methodologies.[25,26] Briefly, samples were pre-enriched in Buffered Peptone Water, selectively enriched in Rappaport–Vassiliadis and Tetrathionate broths, and plated on Xylose Lysine Deoxycholate (XLD) and Hektoen Enteric (HE) agars. Presumptive colonies were confirmed biochemically. All confirmed *Salmonella* isolates were preserved on Nutrient Agar slopes at 4 °C in the Laboratory of Hygiene and Zoonoses, Faculty of Veterinary Medicine, Beni-Suef University, for subsequent analyses.

2.3. Antimicrobial susceptibility testing and MAR index determination

The antimicrobial susceptibility profiles of all *Salmonella* isolates were determined using the standard Kirby–Bauer disk diffusion method, performed in strict compliance with the guidelines of the Clinical and Laboratory Standards Institute.[27] Briefly, 2–3 well-isolated colonies from an overnight culture on Nutrient Agar (NA; Merck, Germany) were emulsified in 5 mL of sterile 0.85% saline to achieve a turbidity equivalent to the 0.5 McFarland standard (approximately 1.5×10^8 CFU mL^{-1}). A sterile cotton swab was dipped into the standardized suspension and used to inoculate the entire surface of a Mueller–Hinton Agar (MHA; Merck, Germany) plate to obtain a confluent lawn of growth. Antibiotic disks ($n = 15$) were aseptically placed on the inoculated plates, which were then incubated at 37 °C for 16–18 hours. The diameters of the inhibition zones (including the disk diameter) were measured to the nearest millimeter using a caliper.

The following antibiotic disks (Oxoid, UK) from eight major classes were tested including β-lactams:ampicillin (AMP, 10 μg), amoxicillin–clavulanate (AMC, 30 μg); cephalosporins:cefoxitin (CX, 30 μg), ceftriaxone (CRO, 30 μg); quinolones/fluoroquinolones:nalidixic acid (NA, 30 μg), ciprofloxacin (CIP, 5 μg), ofloxacin (OFX, 5 μg), enrofloxacin (5 μg); aminoglycosides:gentamicin (GEN, 10 μg), amikacin (AK, 30 μg); sulfonamides:trimethoprim-sulfamethoxazole (COT, 25 μg); tetracyclines:doxycycline (DO, 30 μg); lincosamides:clindamycin (DA, 2 μg); macrolides:erythromycin (ERY, 15 μg); and phosphonic acids:fosfomycin (FO, 200 μg). *Escherichia coli* ATCC 25922 were used as a quality control strain.

The Multiple Antibiotic Resistance (MAR) index was calculated for each isolate using the formula: MAR index = a/b, where 'a' is the number of antibiotics to which the isolate is resistant, and 'b' is the total number of antibiotics tested.[28] Isolates with an MAR index > 0.2 were classified as multidrug-resistant (MDR).[29]

2.4. Molecular detection of antimicrobial resistance genes

2.4.1. Genomic DNA extraction. Genomic DNA was extracted from pure overnight cultures of each *Salmonella* isolate using the QIAamp DNA Mini Kit (Qiagen, Germany) according to the manufacturer's protocol. The concentration and purity of the extracted DNA were assessed using a NanoDrop™ 2000 spectrophotometer (Thermo Fisher Scientific, USA).

2.4.2. Polymerase chain reaction (PCR) amplification. PCR was performed to detect genes conferring resistance to aminoglycosides (**aadA-2**) and fluoroquinolones (*qnrA*). The primer sequences, target amplicon sizes, and specific annealing temperatures are listed in Table 1. Each 25 μL PCR reaction mixture contained 12.5 μL of 2× EmeraldAmp® MAX PCR Master Mix (Takara, Japan), 1 μL of each forward and reverse primer (20 pmol μL^{-1}), 4.5 μL of nuclease-free water, and 6 μL of DNA template (~50 ng). Amplification was carried out in a Veriti™ 96-Well Thermal Cycler (Applied Biosystems, USA) under the following conditions: initial denaturation at 95 °C for 5 min; followed by 35 cycles of denaturation at 95 °C for 30 s, primer annealing at the temperature specified for 45 s, and extension at 72 °C for 45 s; with a final extension at 72 °C for 7 min.

2.4.3. Gel electrophoresis and visualization. The PCR products (10 μL per sample) were mixed with 6× loading dye and separated by electrophoresis on a 1.5% (w/v) agarose gel (Applichem, Germany) prepared in 1× TBE buffer, alongside a 100 bp DNA ladder (GeneRuler, Thermo Scientific). Electrophoresis was performed at a constant voltage of 80 V for 45–60 minutes. The gels were stained with ethidium bromide (0.5 μg mL^{-1}), visualized under ultraviolet light, and photographed using a Gel Documentation System (Alpha Innotech, USA).

Table 1 Primers used for the amplification of antimicrobial resistance genes in *Salmonella* isolates

Target gene	Primer sequence (5′ → 3′)	Amplicon size (bp)	Annealing temp. (°C)	Reference
aadA-2	F: TGTTGGTTACTGTGGCCGTA R: GATCTCGCCTTTCACAAAGC	622	50	30
qnrA	F: ATTTCTCACGCCAGGATTTG R: GATCGGCAAAGGTTAGGTCA	516	52	31

Table 2 Phenotypic and genotypic antimicrobial resistance profiles of *Salmonella* isolates

Sample key	Serovars	Source	No. of antibiotics resistant	Resistance phenotype	MAR index	Resistance genes
1	*S. typhimurium*	Stool	12	CX, GN, EX, DA, NA, OFX, AK, AMP, DO, AMC, CRO, CIP	0.80	*aadA2*, *qnrA*
2	*S. typhimurium*	Bone marrow	11	CX, GN, DA, NA, OFX, AK, AMP, DO, CRO, ERY, CIP	0.73	*aadA2*, *qnrA*
3	*S. typhimurium*	Liver	7	CX, DA, NA, OFX, AK, CIP, AMP	0.47	*aadA2*, *qnrA*
4	*S. enteritidis*	Liver	13	CX, GN, DA, NA, EX, OFX, AK, CIP, AMP, DO, COT, CRO, ERY	0.87	*aadA2*, *qnrA*
5	*S. enteritidis*	Stool	10	CX, GN, DA, NA, DO, AMC, COT, CRO, ERY, CIP	0.67	*aadA2*, *qnrA*
6	*S. infantis*	Intestine	10	GN, DA, AK, AMP, DO, AMC, COT, CRO, ERY, CIP	0.67	*aadA2*, *qnrA*
7	*S. kentucky*	Liver	14	CX, GN, DA, NA, OFX, AK, AMP, DO, AMC, COT, CRO, ERY, FO, CIP	0.93	*aadA2*, *qnrA*
8	*S. virchow*	Gallbladder	9	CX, EX, DA, NA, CIP, AMP, COT, CRO, ERY	0.60	*aadA2*, *qnrA*
9	*S. pensacola*	Liver	10	CX, GN, DA, NA, AK, AMP, DO, CRO, ERY, CIP	0.67	*aadA2*, *qnrA*
10	*S. grampian*	Liver	8	CX, GN, DA, AK, AMP, DO, CRO, ERY	0.53	*aadA2*, *qnrA*
11	*S. kentucky*	Intestine	9	CX, GN, DA, NA, CIP, AMP, COT, CRO, ERY	0.60	*aadA2*, *qnrA*
12	*S. virchow*	Liver	8	CX, GN, DA, AMP, DO, CRO, ERY, CIP	0.53	*aadA2*, *qnrA*
13	*S. gueuletapee*	Liver	9	CX, GN, NA, AK, AMP, DO, CRO, ERY, CIP	0.60	*aadA2*, *qnrA*

2.5. Synthesis and preparation of nanoformulation components

2.5.1. Synthesis of MIL-53(Fe) metal–organic framework. The iron-based metal–organic framework MIL-53(Fe) was synthesized *via* a modified solvothermal method to ensure high crystallinity and purity. In a typical synthesis, iron(III) chloride hexahydrate ($FeCl_3 \cdot 6H_2O$, 5.40 mmol, 1.46 g) and terephthalic acid (H_2BDC, 5.40 mmol, 0.90 g) were dissolved in 50 mL of anhydrous *N*,*N*-dimethylformamide (DMF) under vigorous magnetic stirring for 30 minutes. The homogeneous mixture was then transferred to a 100 mL Teflon-lined stainless-steel autoclave. The sealed autoclave was heated in a programmable oven at 150 °C for 24 hours under autogenous pressure and subsequently allowed to cool naturally to room temperature.[15] The resulting orange-brown crystalline product was recovered by centrifugation at 8000 rpm for 10 minutes and subjected to a rigorous purification protocol to remove unreacted precursors and solvent molecules. This involved three consecutive wash cycles: first with fresh DMF, then with absolute ethanol, and finally with deionized water, each followed by centrifugation. To activate the MOF and evacuate the pores, the washed product was immersed in absolute ethanol for 24 hours, collected, and then dried under vacuum at 120 °C for 12 hours.

2.5.2. Preparation of chitosan solution. A foundational chitosan solution was prepared with precise control over polymer concentration. Low molecular weight chitosan flakes were accurately weighed and gradually added to a 1% (v/v) aqueous acetic acid solution to achieve a final concentration of 0.5% (w/v). Dissolution proceeded under continuous magnetic stirring at 600 rpm and 40 °C for a minimum of 12 hours to ensure complete chain disentanglement, resulting in a clear, viscous, and homogeneous solution. The pH of the final chitosan solution was adjusted to 5.0 ± 0.1 using 1 M sodium hydroxide. This specific pH is critical as it maintains the cationic nature of the chitosan amine groups, which is essential for subsequent ionic cross-linking and antibacterial activity. The solution was filtered through a 0.45 μm syringe filter to remove any undissolved particulates and stored at 4 °C until use within 48 hours.[32,33]

2.5.3. Preparation of drug stock solutions. Individual stock solutions of the active pharmaceutical ingredients were prepared at precise concentrations to ensure accurate dosing during nanoformulation assembly. Gentamicin sulfate was dissolved in 1 : 1 (v/v) mixture of PBS (Phosphate Buffer Saline, pH 7.4) and milliQ water to obtain a clear stock solution of 10 mg mL^{-1}. Ciprofloxacin hydrochloride, due to its limited solubility in water, was first dissolved in a minimal volume of 0.2% acetic acid solution, which was then diluted with deionized water to achieve a final concentration of 5 mg mL^{-1}. Lysozyme was dissolved in 0.2% acetic acid solution to a concentration of 10 mg mL^{-1} to maintain its enzymatic activity and stability. All drug stock solutions were prepared fresh on the day of nanoparticle synthesis, protected from light, and sterilized by filtration through a 0.22 μm membrane filter.

2.5.4. Preparation of sodium tripolyphosphate cross-linking solution. The ionic cross-linker solution was prepared by dissolving sodium tripolyphosphate (TPP) in deionized water to a concentration of 1.0 mg mL^{-1}. The pH of the TPP solution was adjusted to 8.0 using 0.1 M sodium hydroxide to enhance the anionic character of the phosphate groups, thereby optimizing the electrostatic interaction with the protonated amine groups of chitosan during nanoparticle formation. This

solution was also filtered through a 0.22 μm membrane and used immediately.[34,35]

2.6. Quality-by-design optimization and synthesis of the nanoformulation

A systematic Quality-by-Design approach using a three-factor, three-level Box–Behnken Design was employed for optimization *via* Minitab® 21 software. The independent variables were: chitosan concentration (0.5, 1.0, 1.5 mg mL^{-1}), TPP concentration (0.4, 0.7, 1.0 mg mL^{-1}), and MIL-53(Fe) concentration (0.5, 1.5, 2.5 mg mL^{-1}). The critical quality attributes (responses) were: particle size, zeta potential, and the encapsulation efficiency of gentamicin, ciprofloxacin, and lysozyme.[36]

The design generated 17 experimental runs. For each run, hybrid nanoparticles were synthesized *via* an integrated ionic gelation and adsorption method. A specified mass of MIL-53(Fe) was dispersed in the ciprofloxacin solution *via* probe sonication. This suspension was added to the chitosan solution, followed by the addition of gentamicin and lysozyme stocks. After two hours of stirring, nanoparticle formation was induced by the dropwise addition of the TPP solution under vigorous stirring for 60 minutes. The suspension was centrifuged, the pellet was washed and resuspended in deionized water.

2.6.1. Characterization of optimized formulation. The crystalline structure of the prepared materials was analyzed by X-ray diffraction (XRD) using a Bruker D8 Advance diffractometer (Germany) with Cu Kα radiation ($\lambda = 1.5406$ Å) operated at 40 kV and 40 mA over a 2θ range of 5–80°. Functional groups and intermolecular interactions were identified by Fourier transform infrared (FTIR) spectroscopy using a Shimadzu IRSpirit spectrometer (Japan) in the 4000–400 cm^{-1} range with the KBr pellet method.

Surface morphology was examined by field-emission scanning electron microscopy (FE-SEM) using a Zeiss Sigma 500 microscope (Germany), and elemental composition and distribution were determined by energy-dispersive X-ray spectroscopy (EDS) and elemental mapping.

The hydrodynamic particle size, polydispersity index (PDI), size distribution, surface charge, and colloidal stability of the optimized encapsulated formulation were evaluated by Dynamic Light Scattering (DLS) and zeta potential measurements using a Zetasizer Ultra (Malvern Panalytical Ltd, Malvern, UK). All measurements were performed at room temperature.

To ensure accurate particle sizing in the presence of water-soluble drugs (gentamicin and lysozyme), a rigorous sample preparation method was developed. Before DLS measurement, the nanoparticle suspension was subjected to two successive centrifugation-washing cycles at 8000 rpm for 10 minutes to remove any unencapsulated free drug that could potentially interfere with the measurement. After each centrifugation, the supernatant containing free drug was discarded, and the nanoparticle pellet was gently resuspended in fresh deionized water. Control experiments were performed to validate this approach, including DLS measurements of: (i) free drug solutions at concentrations equivalent to those used in the formulation, (ii) empty nanoparticles without drug, and (iii) physical mixtures of empty nanoparticles with free drug. These controls confirmed that free drug solutions produced no detectable scattering signal and that the washing procedure effectively eliminated interference from unencapsulated drug.

For size validation, Transmission Electron Microscopy (TEM) was performed using a JEOL JEM-2100 operating at 200 kV. A drop of the diluted nanoparticle suspension was placed on a carbon-coated copper grid and allowed to adsorb for 2 minutes, after which excess liquid was removed with filter paper. The grid was air-dried at room temperature, and images were captured at various magnifications. A minimum of 200 particles were measured across multiple fields using ImageJ to generate a number-based size distribution and to confirm the morphology of the nanoparticles.

2.6.2. Preparation of the optimized encapsulating formula. The optimal nanoformulation (Encapsulating Formula (EF)) was synthesized as described in Section 2.5 using the following parameters derived from the statistical optimization including chitosan at 1.28 mg mL^{-1}, TPP at 0.41 mg mL^{-1}, and MIL-53(Fe) at 1.89 mg mL^{-1}. The final EF suspension was stored at 4 °C.

The encapsulation efficiency was determined indirectly using an HPLC 1260 Infinity II instrument provided by a quaternary pump, a DAD detector, and an autosampler (Agilent, USA).

Each of ciprofloxacin,[37] lysozyme[38] and gentamicin[39] were quantified by RP-HPLC-DAD in the supernatant separately. EE% was calculated as:

$$EE\% = \left[\frac{W_{\text{initial drug}} - W_{\text{free drug}}}{W_{\text{initial drug}}}\right] \times 100 \quad (1)$$

where $W_{\text{initial drug}}$ is the total mass of the drug added to the formulation, and $W_{\text{free drug}}$ is the mass of the unencapsulated drug detected in the supernatant after centrifugation. This is a standard equation for determining encapsulation efficiency in nanoparticle systems.[40]

2.7. *In vitro* release study and kinetic modeling

This study aimed to quantitatively evaluate and compare the controlled-release capability of the optimized nano-formulation against the rapid release profile of the free, unencapsulated drugs.

2.7.1. Preparation of release medium and test formulations. A phosphate-buffered saline (PBS) medium (0.1 M, pH 7.4) was prepared by dissolving sodium chloride (8.0 g), sodium phosphate monobasic (0.24 g), and sodium phosphate dibasic (1.44 g) in one liter of distilled water. The final pH was adjusted to 7.40 ± 0.05 using 0.1 M solutions of hydrochloric acid or sodium hydroxide.[41] For the comparative release analysis, two distinct test samples were prepared including the Encapsulated Drug Group, consisting of 2 mL of the final optimized chitosan/MIL-53(Fe) nano-formulation suspension, and the Free Drug Group, comprising an aqueous solution containing precise equivalent masses of gentamicin sulfate, ciprofloxacin hydrochloride, and lysozyme. The total drug mass in both samples was standardized to 2 mg.

The release kinetics were assessed simultaneously for both groups using the dialysis bag method under perfect sink

conditions. Regenerated cellulose dialysis bags with a molecular weight cut-off (MWCO) of 14 kDa were pre-hydrated in the PBS medium overnight. The 2 mL volume of each test sample (encapsulated and free) was separately sealed within a dialysis bag. Each bag was then immersed in an individual glass vessel containing 100 mL of the pre-warmed PBS release medium (37.0 ± 0.5 °C). The vessels were placed in a thermostated shaking incubator maintained at a constant agitation of 100 rpm.

Aliquots (1 mL) were withdrawn from the external release medium surrounding each dialysis bag at predetermined time intervals: 5, 15, 30, and 60 minutes, followed by 2, 4, 6, 8, 12, 24, 48, and 72 hours. Immediately after each withdrawal, an equal volume of fresh, pre-warmed PBS was replenished to maintain a constant volume and preserve sink conditions. The collected samples were filtered through a 0.22 μm nylon syringe filter and stored at 4 °C prior to analysis. The concentrations of released ciprofloxacin, gentamicin and lysozyme were determined using validated reverse-phase HPLC-PDA method detailed in Section 2.6.2.

Cumulative release percentages were calculated comparing optimized encapsulated formulation against an unencapsulated one.

Drug release at time t, cumulative drug release (%) were calculated as follow:

$$\text{Released drug at time } t = C_t \times V \tag{2}$$

where, C_t represents the drug concentration at time t (mg mL^{-1}), V represents volume of the dissolution medium (mL).

$$\text{Cumulative drug release}(\%) = \frac{\text{released drug at time } t}{\text{initial amount of drug loaded}} \times 100 \tag{3}$$

The calculation of cumulative drug release is performed according to standard methods for *in vitro* dissolution studies.[42]

2.7.2. Invitro release kinetics. Various release kinetics models were applied including zero-order kinetics (constant release rate),[43] first-order kinetics (release rate depends on the amount of drug remaining),[44] Korsmeyer–Peppas Model (Power Law),[45] Higuchi model (diffusion-controlled release) to give insight into the release mechanism either through diffusion, swelling, or erosion of the encapsulated formulation[46] using the following equations:

$$M_t = M_\infty + k_0 t \tag{4}$$

$$\frac{M_t}{M_\infty} = 1 - e^{-k_1 t} \tag{5}$$

$$\frac{M_t}{M_\infty} = k_{KP} t^n \tag{6}$$

$$M_t = k_H \sqrt{t} \tag{7}$$

M_t = amount of drug released at time t, M_∞ = initial amount of drug, k_0 = zero-order rate constant k_1 = first-order rate constant, n is the release exponent that indicates the release mechanism, t = time, k_{KP} = Korsmeyer–Peppas rate constant, k_H = Higuchi rate constant (depends on properties like the diffusion coefficient, solubility, and surface area).

2.8. Antimicrobial evaluation of the nanoformulation and its components

2.8.1. Preparation of bacterial inoculum. The preserved MDR *Salmonella* isolates were first revitalized by streaking onto Nutrient Agar (NA) plates and incubating at 37 °C for 18–24 hours. Subsequently, a single colony from each isolate was inoculated into 5 mL of Tryptone Soya Broth (TSB; Thermo Fisher Scientific, Code: CM0129B) and incubated at 37 °C for 18 hours with shaking (150 rpm). Following incubation, 3–4 distinct colonies from the fresh NA plates were suspended in sterile 0.85% saline solution, and the turbidity was adjusted to match the 0.5 McFarland standard, yielding a bacterial suspension of approximately 1.5×10^8 colony-forming units per mL (CFU per mL).

2.8.2. Preparation of test materials. The following materials were evaluated for their individual and combined antibacterial activity:

Lysozyme, chitosan (dissolved in 2.0% (v/v) acetic acid), MIL-53(Fe) MOF nanoparticles, gentamicin (pure drug), ciprofloxacin (pure drug), The optimized encapsulating formula (EF) (chitosan/MIL-53(Fe) nanoparticles loaded with gentamicin, ciprofloxacin, and lysozyme).

All compounds, except chitosan, were initially suspended in 10.0% (v/v) dimethyl sulfoxide (DMSO; Oxoid) to prepare primary stock solutions. A working concentration of 1000 μg mL^{-1} for each test material (and the EF) was prepared by further dilution in sterile distilled water. All suspensions were vortexed thoroughly and sonicated for 5 minutes in a Q125 sonicator (125 W, 20 kHz; QSonica, USA) to ensure homogeneity and proper dispersion of nanoparticles.

2.8.3. Agar well diffusion assay. The qualitative antibacterial activity was assessed using the agar well diffusion method as described by Balouiri *et al.* (2016).[47] Briefly, 15 mL of sterilized Mueller–Hinton Agar (MHA) was poured into sterile Petri dishes and allowed to solidify. The standardized bacterial suspension (1.5×10^8 CFU mL^{-1}) was swabbed uniformly over the entire surface of the agar plates using a sterile cotton swab. Wells of 6 mm diameter were aseptically punched into the inoculated agar using a sterile micropipette tip. Subsequently, 40 μL of each test material (1000 μg mL^{-1}) or the EF was carefully dispensed into individual wells. The plates were allowed to stand at room temperature for 45 minutes to permit pre-diffusion of the agents, and then incubated at 37 °C for 24 hours. The diameters (in mm) of the resulting inhibition zones, including the well diameter, were measured using a digital caliper. Each assay was performed in triplicate for each bacterial isolate, and the results are expressed as mean ± standard error of the mean (SEM).

2.8.4. Determination of minimum inhibitory concentration (MIC) and minimum bactericidal concentration (MBC). The quantitative antibacterial efficacy was determined using the

standard broth macrodilution method in accordance with CLSI guidelines.[48] Two-fold serial dilutions of each test material and the EF were prepared in Brain Heart Infusion (BHI) broth (Oxoid, UK) across a concentration range of 500 μg mL^{-1} to 0.156 μg mL^{-1} in sterile test tubes. Each tube was inoculated with an adjusted bacterial suspension to achieve a final inoculum density of approximately 1.5×10^5 CFU mL^{-1} (derived from a 1 : 100 dilution of the 0.5 McFarland standard). The tubes were incubated at 37 °C for 24 hours. The MIC was recorded as the lowest concentration of the agent that completely inhibited visible bacterial growth.

To determine the MBC, 50 μL aliquots from tubes showing no visible growth (including the MIC tube and concentrations above it) were subcultured onto fresh BHI agar plates. The plates were incubated at 37 °C for 24 hours. The MBC was defined as the lowest concentration of the agent that resulted in ≥99.9% killing of the initial inoculum (*i.e.*, no growth on subculture).[49] Sterile, non-inoculated BHI broth served as a negative control, and inoculated BHI broth without any antimicrobial agent served as a positive control. All tests were performed in triplicate. The MBC/MIC ratio was calculated to determine the nature of the antibacterial activity: a ratio of ≤4 was considered bactericidal, while a ratio of >4 indicated bacteriostatic activity.

2.8.5. Assessment of synergistic effect. The synergistic effect of the combined components within the optimized EF was quantitatively evaluated using the Fractional Inhibitory Concentration (FIC) index.[50] The FIC for each individual component in the combination was calculated as follows:

$$FIC_X = \frac{MIC_{EF}}{MIC_X}$$

where MIC_{EF} is the MIC of the complete encapsulating formula, and MIC_X is the MIC of component X (L: Lysozyme, M: MIL-53(Fe), C: Chitosan, CIP: Ciprofloxacin, GEN: Gentamicin) when tested alone.

The FIC Index (FICI) was then determined as the sum of the individual FIC values for all components:

$$FICI = \sum FIC_X$$

The interaction was interpreted as follows: synergy (FICI ≤ 0.5), additivity (0.5 < FICI ≤ 1), indifference (1 < FICI ≤ 4), or antagonism (FICI > 4).

2.8.6. Statistical analysis. The antibacterial activity data (inhibition zones, MICs, MBCs) were analyzed using one-way Analysis of Variance (ANOVA) followed by Tukey's *post hoc* test for multiple comparisons. All statistical analyses were performed using SPSS software (Version 22.0; IBM Corp., USA). Data are presented as mean ± SEM. A probability value (p) of less than 0.05 was considered statistically significant.

2.9. Computational docking analysis

To gain a molecular-level understanding of the potential interactions between the nanoformulation components and a key bacterial virulence factor, computational docking was performed against the SipD protein (PDB: 2YM9) from *Salmonella typhimurium*. SipD is a critical component of the Type III secretion system (T3SS) injectisome, essential for host cell invasion.

The three-dimensional structures of the ligands were modeled using the Molecular Operating Environment software (MOE, 2015.10). The ligands included: ciprofloxacin, gentamicin, D-glucosamine (the repeating monomeric unit of chitosan), and terephthalic acid (the organic linker of MIL-53). Florfenicol was used as a reference control drug.

The crystal structure of SipD (2YM9) was prepared for docking using the Protonate 3D protocol in MOE. All water molecules were removed, and hydrogen atoms were added. The co-crystallized ligand was used to define the active binding site. The docking protocol was validated by re-docking the native ligand, yielding a root-mean-square deviation (RMSD) of <2.0 Å, confirming the reliability of the method.

Docking simulations were performed using the Triangle Matcher placement method and the London dG scoring function. For each compound, the pose with the most favorable (most negative) docking score (kcal mol^{-1}) was selected. The specific interactions (hydrogen bonds, ionic bonds, *etc.*) between the ligand and key amino acid residues in the SipD binding pocket were analyzed and visualized using MOE and BIOVIA Discovery Studio Visualizer.[51,52]

3 Results and discussion

3.1. Phenotypic and genotypic characterization of MDR *Salmonella* isolates

Thirteen *Salmonella* isolates, encompassing eight epidemiologically significant serovars (Typhimurium, Enteritidis, Infantis, Virchow, Kentucky, Peniscola, Grampian, and Gueuletapee) from poultry and clinical sources, demonstrated extensive antimicrobial resistance. All isolates exhibited multidrug-resistant (MDR) phenotypes, with *S. kentucky* displaying the broadest spectrum, being resistant to 14 of the 15 tested antibiotics across eight classes (Table 2). Critically, 100% of isolates showed phenotypic resistance to both gentamicin and ciprofloxacin. This resistance was genotypically corroborated by the universal detection of the aminoglycoside resistance gene **aadA*-2* (622 bp) and the plasmid-mediated quinolone resistance gene *qnrA* (516 bp), as shown in Fig. 1. The average Multiple Antibiotic Resistance (MAR) index was 0.58 (range: 0.53–0.93), with values >0.7 for several isolates indicating origin from environments with intensive, non-therapeutic antibiotic use.

Several studies studied the drug resistance pattern of *Salmonella* including; Chea *et al.* (2025) in Cambodia,[53] who reported a significantly MDR of *Salmonella* isolates of poultry for three to five antimicrobial classes including a moderate resistance against fluoroquinolones, and lower resistance against aminoglycosides whereas, higher pattern of resistance against β-lactams, tetracyclines, and sulfonamides. Also, Basuony *et al.* (2024),[54] in Egypt investigated that the majority *Salmonella* serovars from poultry internal organs revealed resistant to at least three antimicrobial drugs from various antimicrobial classes with an extreme resistance against

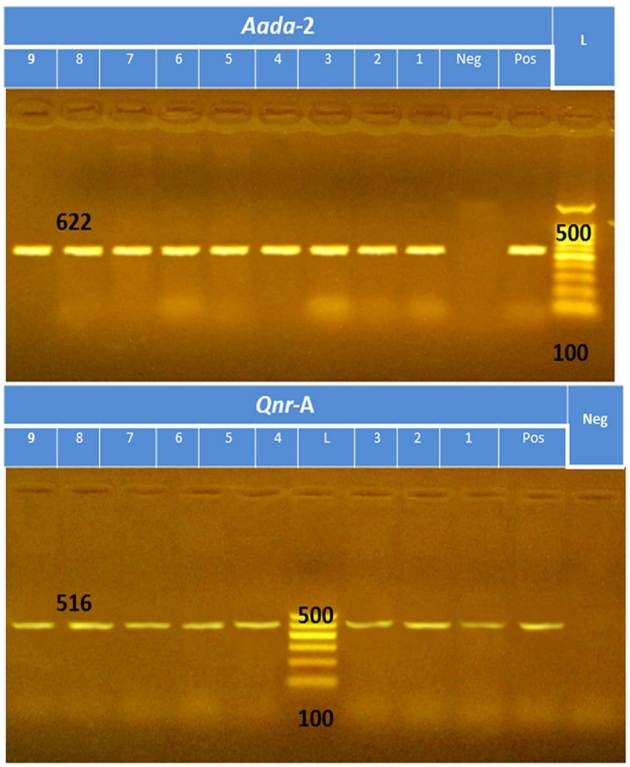

Fig. 1 Molecular detection of *aadA-2* and *qnrA* resistance genes. Representative agarose gel image of PCR products from *Salmonella* isolates shows specific amplicons for the aminoglycoside resistance gene *aadA-2* (622 bp) and the quinolone resistance gene *qnrA* (516 bp). Lane L: 100 bp DNA ladder; Neg: negative control; Pos: positive control; lanes 1–9: tested *Salmonella* isolates.

ampicillin and clindamycin, and variable resistance pattern against gentamicin, ciprofloxacin, cefotaxime, tetracycline, and amakicin with MAR indices ranged from 0.214 to 0.786. Also, Abdel-Maksoud *et al.* (2015) in Egypt reported that poultry samples exhibited a high rate of drug resistance against ampicillin, tetracycline, sulphamethoxazole, and nalidixic acid.[55] Besides, Kanu *et al.*(2024),[56] who reported that *S. Typhimurium* from poultry origins emphasized a high resistant rates to ampicillin, ceftazidime and chloramphenicol, cefuroxime, cefotaxime, sulphamethoxazole/trimethoprim and amoxicillin–clavulanic acid but less resistant to gentamicin, ofloxacin, ciprofloxacin and they recorded MAR indices of 0.8 values.

Also, Muhammed *et al.* (2010) reported that *Salmonella* isolate from a poultry farm in Jos, Nigeria was resistant to gentamicin and ciprofloxacin.[57] However, Rushdy *et al.* (2013) reported that 58 *Salmonella* isolates, showed resistance to most tested antibiotics especially the fluoroquinolone group[58] where *S. Typhimurium* was resistant to all tested 20 antibiotics namely: aminoglycosides group (gentamycin and amikacin), β-lactams group (ampicillin, ampicillin/sulbactam, amoxicillin/clavulanic acid, piperacillin, piperacillin/tazobactam, cefotaxime, ceftriaxone, ceftazidime, cefepime, imipenem, aztreonam), phenicols (chloramphenicol), sulfa drug group (sulfamethazine), and *Enteritidis* emphasized a resistant indicators to the same antibiotic categories except sulfamethoxazole trimethoprim.

Antimicrobials are widely utilized in chicken production for therapy, prophylaxis, metaphylaxis, and growth promotion (Boeckel *et al.* 2015).[59] The most regularly used antimicrobials are β-lactams, tetracyclines, sulfonamides, aminoglycosides, and fluoroquinolones. Furthermore, around 80.0% of animals used for food production, including poultry are administrated antibiotics at all points in their lives. This raises the possibility that antibiotic residues will be detected in edible organs especially liver in its patent forms promote carcinogenicity, mutagenicity, bone marrow toxicity, and propagation drug resistance throughout the food chain. Additionally, Khalafalla *et al.* (2022) in Egypt reported that 60.0% of the chicken meat samples included antibiotic residues, namely for enrofloxacin, oxytetracycline, and sulfadimidine.[60] Also, the widespread and inappropriate use of antimicrobials has contributed to the establishment and dissemination of resistance genotypes among enteric bacteria, including *Salmonella* (Cao *et al.*, 2020),[61] especially through mobile elements such as plasmids transfer among various microbial species. These findings highlight the potential risks associated with AMR transmission in the food chain and emphasize the necessity of the urgent surveillance and the immediate intervention strategies to control AMR in animals.

The universal co-occurrence of resistance to these critically important antimicrobials, mediated by mobile genetic elements, presents a severe therapeutic challenge and underscores a significant zoonotic risk. This finding provided the imperative for developing an advanced delivery system capable of overcoming these specific resistance mechanisms.

3.2. Quality-by-design optimization of the hybrid nanoformulation

A Quality-by-Design (QbD) approach, employing a three-factor, three-level Box–Behnken Design (BBD), was implemented to rationally engineer the hybrid nanoformulation. The independent variables were chitosan concentration (*A*: 0.5–1.5 mg mL^{-1}), sodium tripolyphosphate (TPP) concentration (*B*: 0.4–1.0 mg mL^{-1}), and MIL-53(Fe) concentration (*C*: 0.5–2.5 mg mL^{-1}). The critical quality attributes (CQAs) defined for optimization were particle size (Y_1), zeta potential (Y_2), and the encapsulation efficiency (EE%) of gentamicin (Y_3), ciprofloxacin (Y_4), and lysozyme (Y_5).

The experimental data from 17 runs were fitted to quadratic models. Analysis of Variance (ANOVA) confirmed the high statistical significance ($p < 0.0001$) and adequacy of all models. The final polynomial equations in terms of coded factors are presented below, where positive coefficients indicate a synergistic effect and negative coefficients indicate an antagonistic effect on the response:

$$\text{Particle size (nm): } Y_1 = 195.0 + 52.5A + 7.5B + 25.0C + 26.0A^2 + 6.0B^2 + 11.5C^2$$

$$\text{Zeta potential (mV): } Y_2 = 31.0 - 2.0A - 7.0B - 1.0C - 1.0A^2 - 1.0B^2$$

$$\text{EE\% gentamicin: } Y_3 = 64.0 + 7.0A - 8.0B + 1.0C - 1.0A^2 - 3.0B^2 - 1.0C^2$$

$$\text{EE\% ciprofloxacin: } Y_4 = 76.0 + 1.0A - 0.5B + 12.5C + 0.5A^2 + 1.0C^2$$

$$\text{EE\% lysozyme: } Y_5 = 38.0 + 6.0A - 3.0B + 3.0C + 1.5A^2 - 1.5B^2 - 0.5C^2$$

The ANOVA results, summarized in Table S1, provide detailed statistical validation for each model. The exceptionally low p-values ($p < 0.0001$) and high R^2 values confirm that the models are highly significant and explain a great majority of the variability in the data. The close agreement between the adjusted R^2 and predicted R^2 values supports the models' robustness for prediction. This statistical validation confirms that the derived polynomial equations are reliable tools for understanding factor effects.

The models served as a precise diagnostic tool, quantifying the influence of each factor and their interactions on the CQAs. These relationships were further visualized through three-dimensional response surface and two-dimensional contour plots (Fig. 2–6), which were critical for interpreting the complex design space. Particle size (Fig. 2) was predominantly and positively influenced by chitosan concentration (linear coefficient: +52.5), consistent with its role as the primary polymeric matrix determining nanoparticle growth. A notable positive interaction with MIL-53(Fe) concentration was also observed. Zeta potential (Fig. 3) was most strongly and negatively affected by TPP concentration (coefficient: −7.0). This is attributed to the neutralization of the cationic chitosan amine groups by the anionic cross-linker, underscoring the need to optimize TPP levels to maintain sufficient positive charge for colloidal stability.

Regarding encapsulation efficiency, the models revealed distinct loading mechanisms. Gentamicin EE% (Fig. 4) was favorably influenced by chitosan (+7.0) but strongly hindered by TPP (−8.0), suggesting entrapment within the chitosan matrix that is compromised by excessive cross-linking. In stark contrast, ciprofloxacin EE% (Fig. 5) was overwhelmingly dependent on MIL-53(Fe) concentration (+12.5), providing quantitative proof of its primary adsorption into the MOF's porous architecture *via* π–π stacking and coordination interactions. Lysozyme EE% (Fig. 6) showed a dual dependency, with positive effects from both chitosan (+6.0) and the MOF (+3.0).

Guided by the statistical models and their visual representations in Fig. 2–6, a multi-response numerical optimization was performed. The goal was to identify the factor levels that simultaneously minimized particle size, maximized zeta potential, and maximized the EE% of all three active agents.

This analysis yielded the definitive optimal formulation parameters: chitosan at 1.28 mg mL^{-1}, TPP at 0.41 mg mL^{-1}, and MIL-53(Fe) at 1.89 mg mL^{-1}.

To confirm the reliability of the quadratic models and ensure that the predicted optimal formulation could be reproduced experimentally, validation runs were performed in triplicate at the optimal factor levels. The experimental values for all five responses were within 2.5% of the model predictions (particle size: 248 ± 11 nm *vs.* 242.5 nm predicted; zeta potential: +33.8 ± 1.7 mV *vs.* +34.2 mV predicted; EE% gentamicin: 68.5 ± 2.4% *vs.* 69.3% predicted; EE% ciprofloxacin: 85.1 ± 1.9% *vs.* 86.0% predicted; EE% lysozyme: 39.7 ± 2.1% *vs.* 40.5% predicted). All experimental results fell within the 95% prediction intervals calculated by the software. Residual analysis confirmed normality and constant variance, and the low coefficients of variation (% CV < 6%) across triplicate runs demonstrated good reproducibility. These results confirm that the QbD approach successfully identified a robust formulation region and that the predicted data are accurate and achievable under laboratory conditions.

3.3. Characterization of the optimized nanoformulation

The XRD patterns of the prepared materials are shown in Fig. 7a. Pristine chitosan exhibits a broad diffraction peak at $2\theta \approx 19.9°$, characteristic of its semi-crystalline nature, which originates from hydrogen bonding between polymer chains. In the composite, distinct peaks corresponding to the crystalline metal–organic framework MIL-53(Fe) are observed at low angles ($2\theta \approx 10.7°$ and 11.5°), which align with reported literature.[62,63] Specifically, the peaks at $2\theta = 11.5°$ and 19.6° are conclusively assigned to the (200) and (−110) crystallographic planes of MIL-53(Fe), respectively.[64] The presence of these MIL-53(Fe) peaks and the simultaneous absence of other major phases in the composite confirm that the framework's crystal structure is preserved following its incorporation into the chitosan matrix and subsequent loading with biomolecules and drugs.

Furthermore, an intense diffraction peak at $2\theta \approx 72°$ is attributed to highly crystalline iron oxide phases, likely formed from a partial structural transformation of MIL-53(Fe). The persistence and sharpness of this peak indicate the presence of well-ordered Fe–O domains embedded within the chitosan-based hybrid matrix.[65] The lack of sharp diffraction features for lysozyme and the loaded drugs (ciprofloxacin and gentamicin) suggests they are in an amorphous state when immobilized within the polymeric/porous composite, which is indicative of successful encapsulation or surface immobilization—a state often favorable for biological activity.

FTIR spectroscopy was conducted to identify the functional groups present in the prepared biomaterials (Fig. 7b). The spectrum for pure lysozyme (Lys) displays characteristic protein bands: a broad band at 3293 cm^{-1} (overlapping O–H and N–H stretches), a peak at 1652 cm^{-1} (amide I, C=O stretch), and a peak at 1534 cm^{-1} (amide II, N–H bend).[66]

The spectrum of pristine chitosan (Ch) shows a broad peak between 3442 and 3142 cm^{-1}, attributed to –OH and –NH$_2$ stretching vibrations and surface-bound water. Absorption peaks at 1642 cm^{-1} and 1402 cm^{-1} are assigned to the carbonyl (C=O) stretch and amine deformation mode, respectively.[67] Very weak peaks near 2932 and 2859 cm^{-1} are likely linked to C–H stretching in the glucosamine units.[68]

The FTIR results for the final composite clearly demonstrate the successful fabrication of a multifunctional Ch/MIL-53

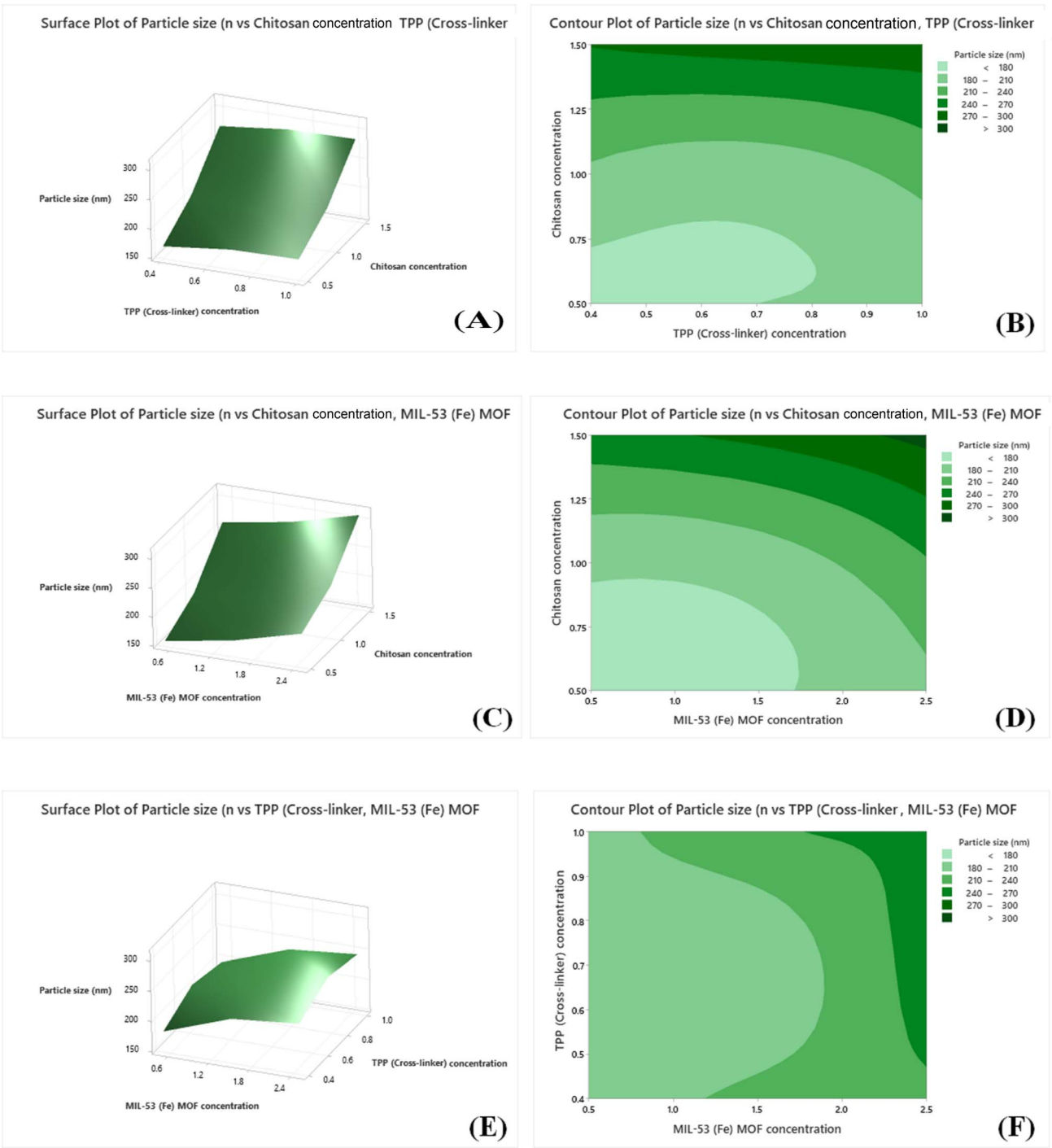

Fig. 2 Response surface (3D) and contour (2D) plots showing the interactive effects of formulation variables on nanoparticle particle size (Y_1). (A) Response surface and (B) contour plot of chitosan (A) and TPP (B) at fixed MIL-53(Fe) (C, center level). (C) Response surface and (D) contour plot of chitosan (A) and MIL-53(Fe) (C) at fixed TPP (B, center level). (E) Response surface and (F) contour plot of TPP (B) and MIL-53(Fe) (C) at fixed chitosan (A, center level).

material loaded with Lys, ciprofloxacin (CIP), and gentamicin (Gent). The observed band shifts and broadening in the composite spectrum confirm strong intermolecular interactions (*e.g.*, hydrogen bonding, electrostatic) during the loading process. These interactions support the enhanced stability and suitability of the composite for controlled antimicrobial or biomedical applications.

The FE-SEM micrographs of the Ch/MOF composite are presented in Fig. 8(a and b). At low magnification (Fig. 8a), the morphology reveals a heterogeneous surface where MIL-53 nanocrystals are evenly distributed and enveloped by a closely

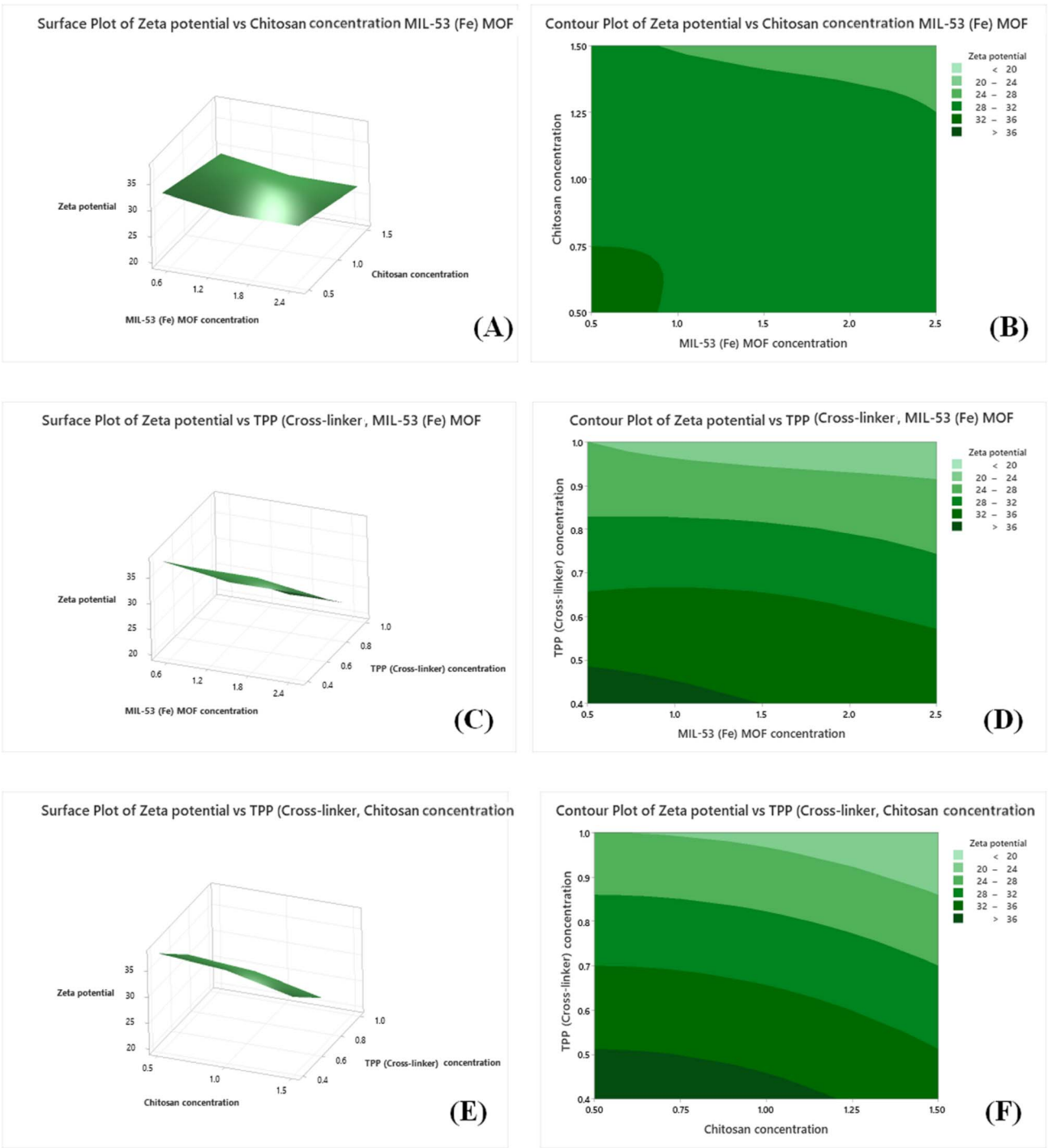

Fig. 3 Response surface (3D) and contour (2D) plots illustrating the interactive effects of formulation variables on nanoparticle zeta potential (Y_2). (A) Response surface and (B) contour plot of chitosan (A) and MIL-53(Fe) (C) at fixed TPP (B, center level). (C) Response surface and (D) contour plot of TPP (B) and MIL-53(Fe) (C) at fixed chitosan (A, center level). (E) Response surface and (F) contour plot of chitosan (A) and TPP (B) at fixed MIL-53(Fe) (C, center level).

connected polymeric film, due to hydrogen bonding between chitosan and the MOF.[69,70] Higher magnification (Fig. 8b) clearly shows characteristic rod- or needle-like crystals, confirming the successful growth of MIL-53 frameworks. These micro-rods are randomly oriented and densely distributed. The chitosan polymer appears as an irregular, rough, and agglomerated background matrix that embeds and anchors the MOF crystals, indicating good interfacial interaction.

Images of the drug-loaded sample (Ch/MOF/Lys/Gent/CIP) in Fig. 8(c and d) show that the incorporated drugs are well-dispersed within the material's pores. The observed surface roughness and particle clustering support successful drug

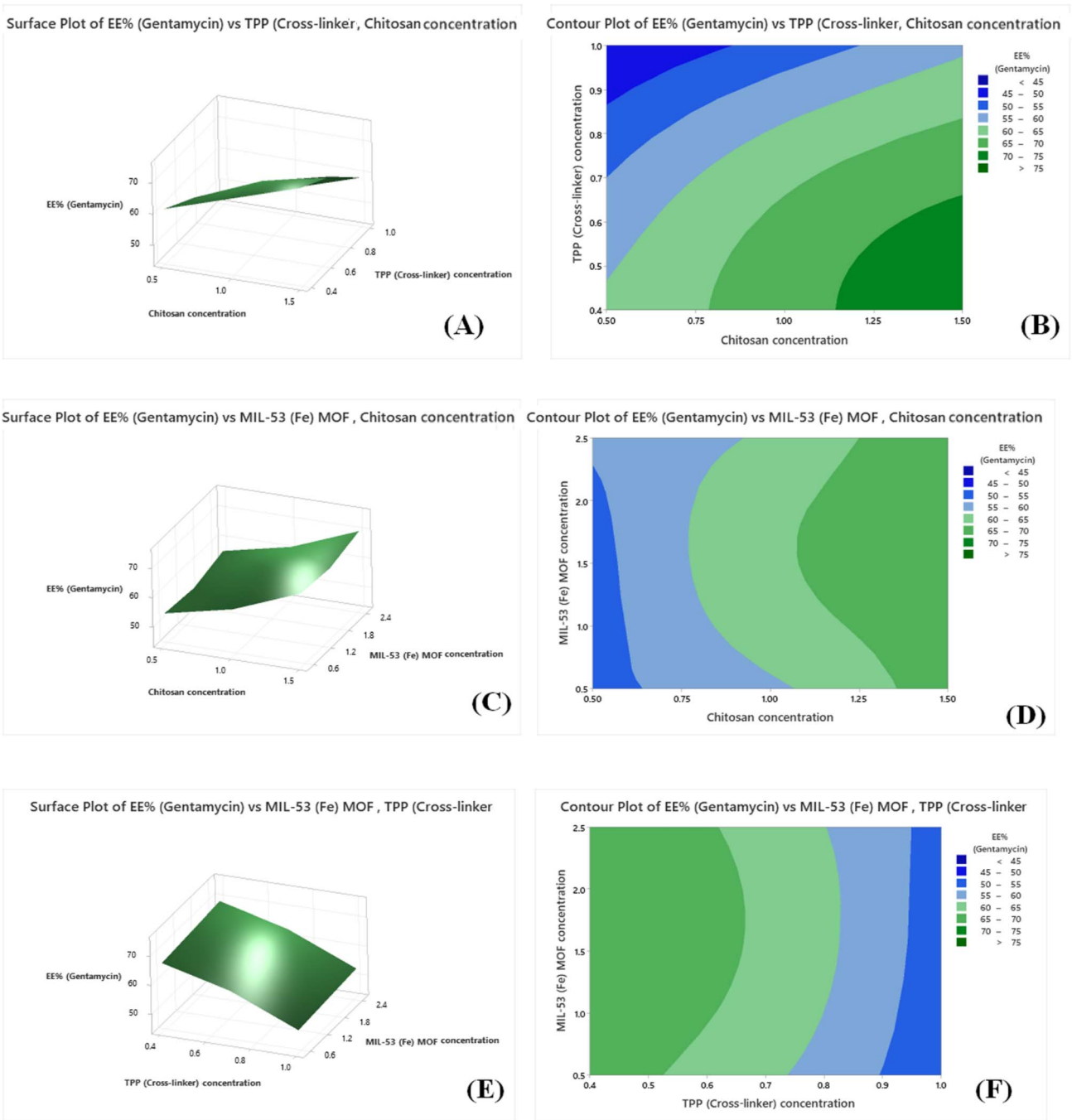

Fig. 4 Response surface (3D) and contour (2D) plots illustrating the interactive effects of formulation variables on the encapsulation efficiency (EE%) of gentamicin (Y_3). (A) Response surface and (B) contour plot of chitosan (A) and TPP (B) at fixed MIL-53(Fe) (C, center level). (C) Response surface and (D) contour plot of chitosan (A) and MIL-53(Fe) (C) at fixed TPP (B, center level). (E) Response surface and (F) contour plot of TPP (B) and MIL-53(Fe) (C) at fixed chitosan (A, center level).

incorporation and encapsulation within a porous structure formed by thin Ch/MOF walls. The final material's porous architecture, comprising random and irregular macropores, is conditioned by the properties of the precursor solutions and the loading conditions.[71–73]

The elemental composition and distribution were analyzed by EDX and mapping (Fig. 8e–i). The images demonstrate a homogeneous distribution of iron (Fe), nitrogen (N), and carbon (C) throughout the matrix. This uniformity confirms the effective integration of MIL-53(Fe) and the consistent loading of ciprofloxacin, gentamicin, and lysozyme within the chitosan scaffold. Such homogeneity is critical for achieving enhanced material stability, controlled drug release, and synergistic antimicrobial performance.

Nanoparticles synthesized at the optimal point exhibited excellent characteristics (Table S2). Particle size analysis was

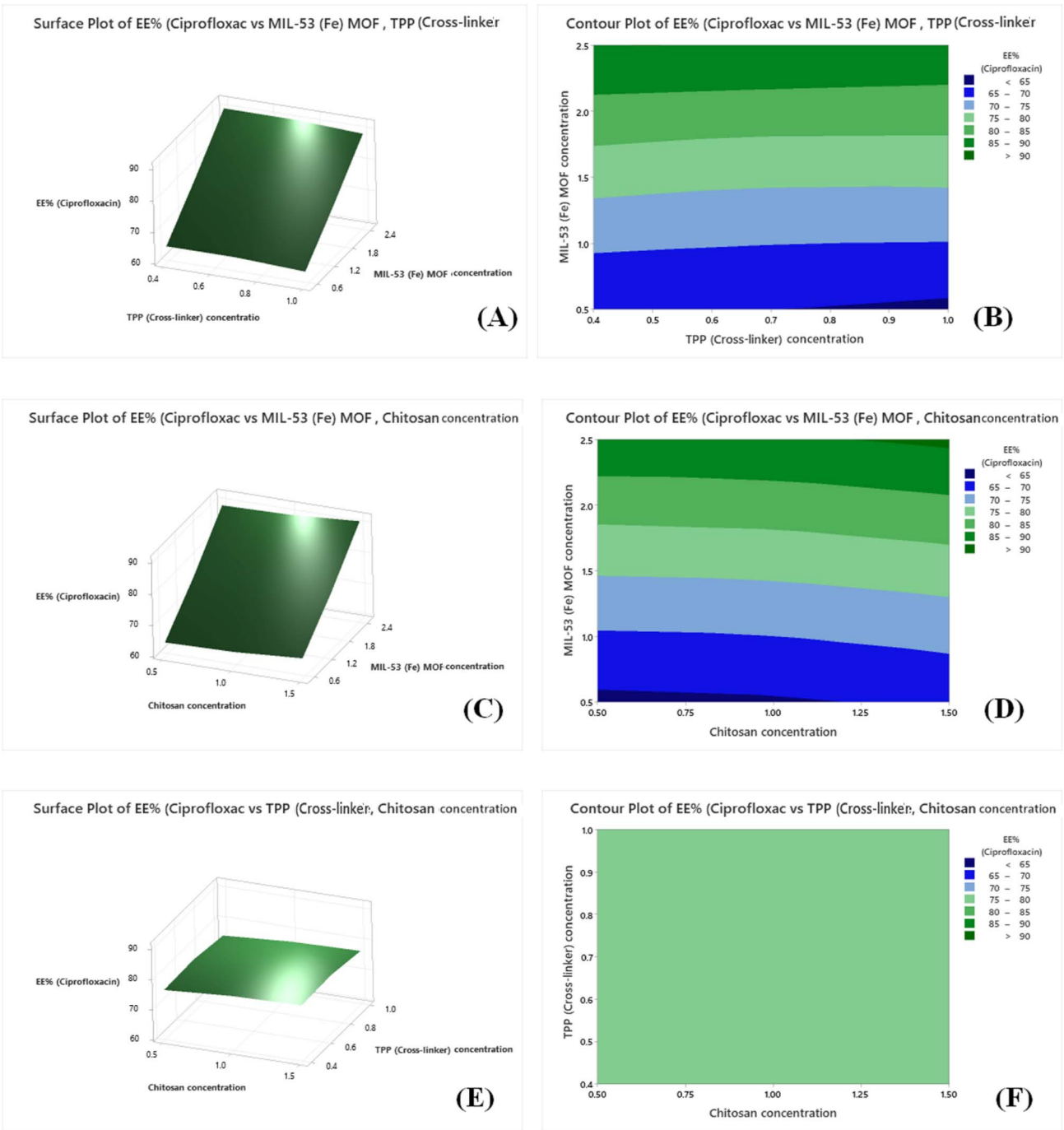

Fig. 5 Response surface (3D) and contour (2D) plots illustrating the interactive effects of formulation variables on the encapsulation efficiency (EE%) of ciprofloxacin (Y_4). (A) Response surface and (B) contour plot of MIL-53(Fe) (C) and TPP (B) at fixed chitosan (A, center level). (C) Response surface and (D) contour plot of MIL-53(Fe) (C) and chitosan (A) at fixed TPP (B, center level). (E) Response surface and (F) contour plot of TPP (B) and chitosan (A) at fixed MIL-53(Fe) (C, center level).

performed using Dynamic Light Scattering (DLS) with a Malvern Zetasizer Ultra. To ensure accurate particle sizing in the presence of water-soluble drugs (gentamicin and lysozyme), a rigorous sample preparation method was developed. Before DLS measurement, the nanoparticle suspension was subjected to two successive centrifugation-washing cycles (8000 rpm, 10 minutes) to remove any unencapsulated free drug that could potentially interfere with the measurement. The supernatant was discarded, and the pellet was resuspended in deionized water after each wash. Control experiments confirmed that free drug solutions at equivalent concentrations produced no detectable scattering signal, and that physical mixtures of empty nanoparticles and free drug exhibited bimodal distributions, validating the necessity and effectiveness of the

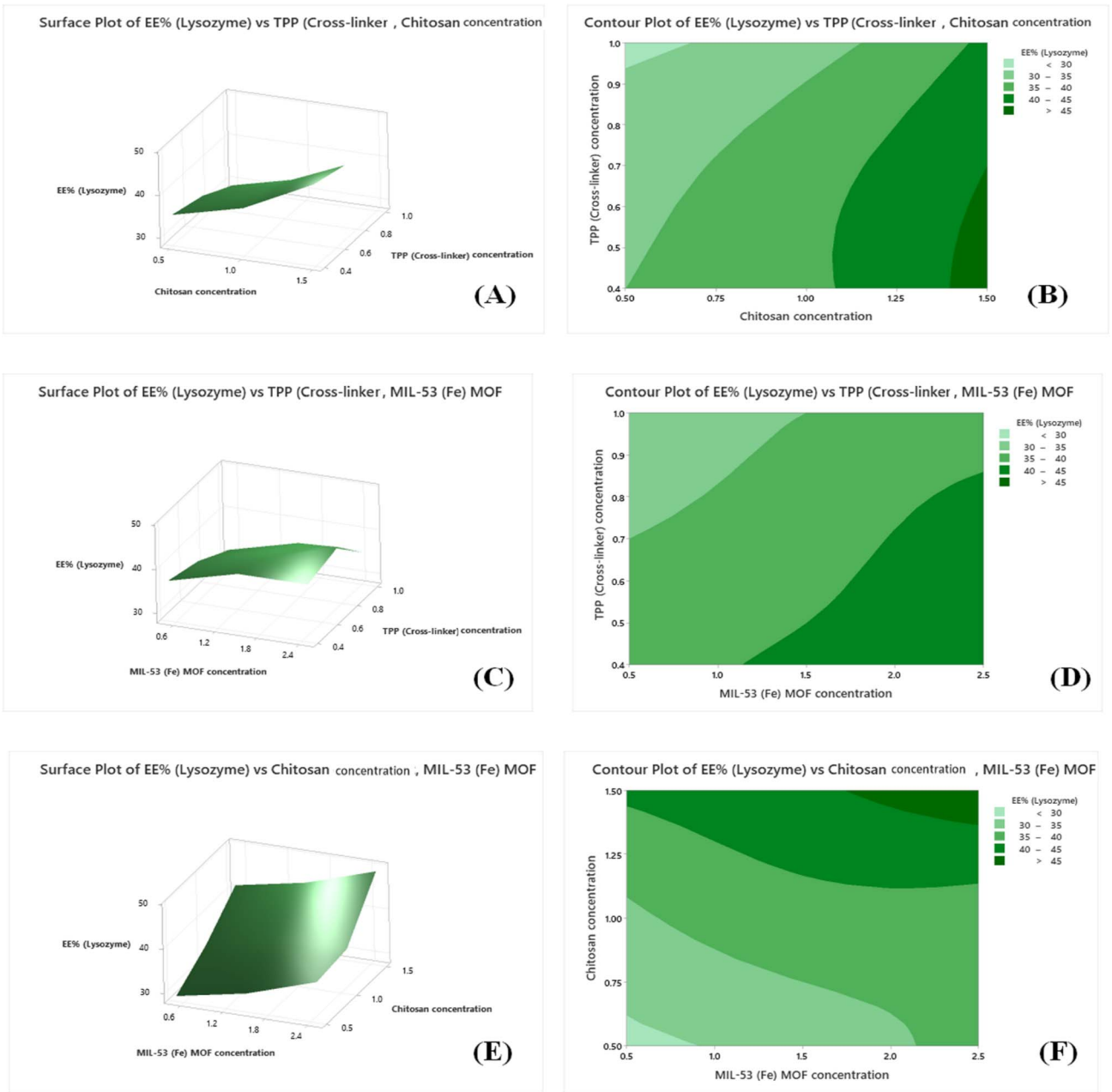

Fig. 6 Response surface (3D) and contour (2D) plots illustrating the interactive effects of formulation variables on the encapsulation efficiency (EE%) of lysozyme (Y_5). (A) Response surface and (B) contour plot of chitosan (A) and TPP (B) at fixed MIL-53(Fe) (C, center level). (C) Response surface and (D) contour plot of TPP (B) and MIL-53(Fe) (C) at fixed chitosan (A, center level). (E) Response surface and (F) contour plot of chitosan (A) and MIL-53(Fe) (C) at fixed TPP (B, center level).

washing procedure. Encapsulation efficiency measurements (68.5% for gentamicin, 85.1% for ciprofloxacin, 39.7% for lysozyme) further confirmed that the majority of the drug was associated with the nanoparticles rather than free in solution.

Following this washing procedure, DLS measurements were performed on properly diluted samples (100-fold in filtered deionized water) at 25 °C with a backscattering angle of 173°. Each measurement comprised 12–15 runs, and results represent the mean of three independent measurements ($n = 3$). The derived count rate remained stable at 285.6 ± 12.4 kcps with an optimized attenuator index of 7–8, and the correlation functions exhibited smooth, single-exponential decay with clean baselines, confirming the absence of aggregation or dust contamination. The reported value of 248 ± 11 nm represents the *Z*-average hydrodynamic diameter, which is the intensity-weighted mean size and the standard reporting parameter for DLS according to ISO 22412:2017. The Polydispersity Index (PDI) was 0.21 ± 0.02, indicating a narrow and relatively monodisperse size distribution. The low coefficient of variation

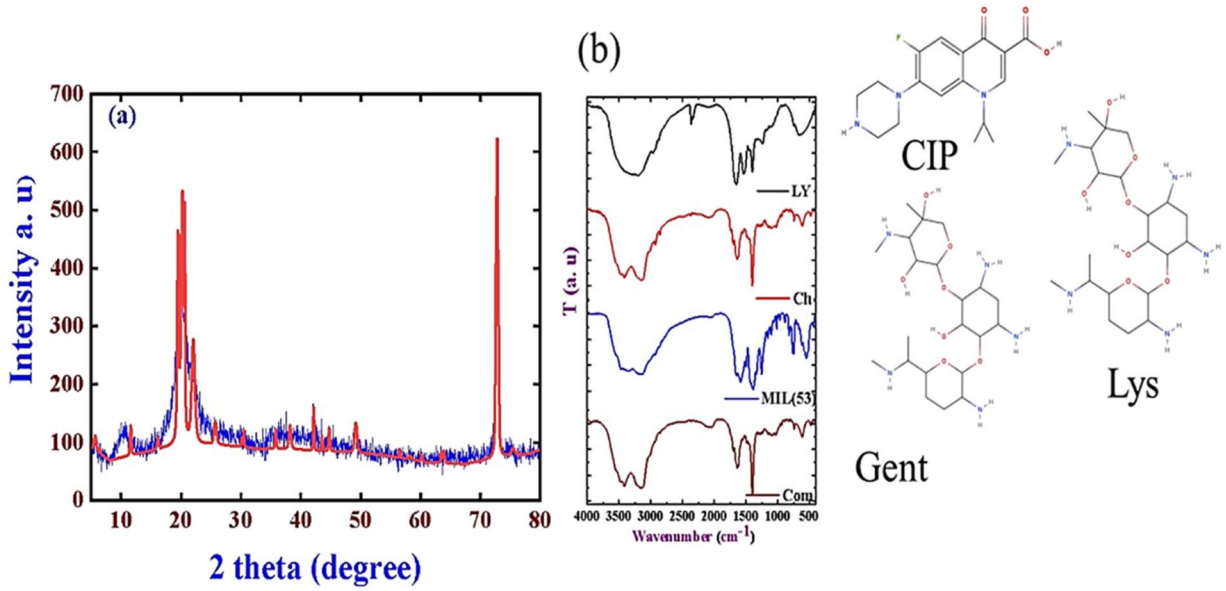

Fig. 7 (a) XRD patterns of the pristine materials and the prepared composite. (b) FTIR spectra of Lys, MIL-53(Fe), Ch, and the composite. The inset shows the chemical structures of CIP, Gent, and Lys.

(<5%) across replicate measurements further validated the reproducibility and reliability of the size data.

To provide orthogonal validation of the particle size, Transmission Electron Microscopy (TEM) was performed on the optimized formulation. TEM imaging revealed spherical nanoparticles with measured core diameters of approximately 210 nm and 230 nm (Fig. 8j and k, indicated by arrows). This closely agrees with the DLS hydrodynamic diameter of 248 nm. The slight discrepancy (approximately 15%) is expected and well-documented, as DLS measures the hydrated particle including the polymer corona and solvation layer, while TEM measures the dried core in a vacuum. The close agreement between these two independent techniques confirms the reliability of both methods and validates the particle size determination.

Collectively, these multiple lines of evidence, including rigorous washing to remove free drug, stable DLS measurement parameters, reproducible correlation functions, low coefficient of variation, and independent TEM validation confirm that the sharp size distribution observed in Fig. 8l authentically represents a highly monodisperse nanoparticle population achieved through the optimized Quality-by-Design formulation parameters, rather than measurement artifacts or free drug interference.

The high positive zeta potential of +33.8 ± 1.7 mV ensures strong electrostatic repulsion between particles, predicting superior colloidal stability and prolonged shelf-life, as shown in Fig. 8l and m. Most critically, the formulation achieved efficient co-encapsulation of all three antimicrobials: 68.5 ± 2.4% for gentamicin, 85.1 ± 1.9% for ciprofloxacin, and 39.7 ± 2.1% for lysozyme. The high EE% for ciprofloxacin directly validates the model's prediction of MIL-53(Fe)-driven loading.

The successful application of QbD and RSM transformed the formulation from an empirical trial-and-error process into a rational engineering exercise. It quantitatively elucidated the complex interactions between components, allowing for the deliberate creation of a nano-platform with predefined, optimal properties tailored for multi-agent delivery.

3.4. Molecular docking analysis predicts interactions with a virulence-associated target

To complement the physico-chemical and biological evaluations and provide a molecular-level rationale for the observed synergistic efficacy, *in silico* molecular docking was performed against the SipD protein (PDB: 2YM9) from *Salmonella typhimurium*. SipD is a critical component of the Type III secretion system (T3SS) injectisome, essential for host cell invasion. Targeting this virulence factor represents a potential strategy to disarm the pathogen in addition to killing it.

The docking results, summarized in Table 3, revealed distinct binding affinities for the components of our nanoformulation compared to the reference drug florfenicol. Florfenicol exhibited a docking score of −4.51 kcal mol^{-1}, interacting moderately with Lys182 and Lys188 (Fig. 9A). In contrast, the antibiotic payloads of our system demonstrated superior predicted binding. Ciprofloxacin docked with a score of −4.96 kcal mol^{-1}, forming an extensive network of hydrogen and ionic bonds with critical residues, including Glu237, Lys182, Lys188, and Lys276 (Fig. 9B). Most notably, gentamicin demonstrated the strongest binding affinity among all tested compounds, with a score of −5.58 kcal mol^{-1}. Its complex was stabilized by a robust hydrogen-bonding network involving Ser236, Glu237, Gln233, Ser278, and Glu281, alongside key ionic interactions (Fig. 9C). This suggests that, beyond their primary mechanisms of action (DNA gyrase inhibition and ribosomal targeting, respectively), these antibiotics may possess a secondary, previously underappreciated capacity to interfere with the T3SS virulence apparatus by binding to SipD.

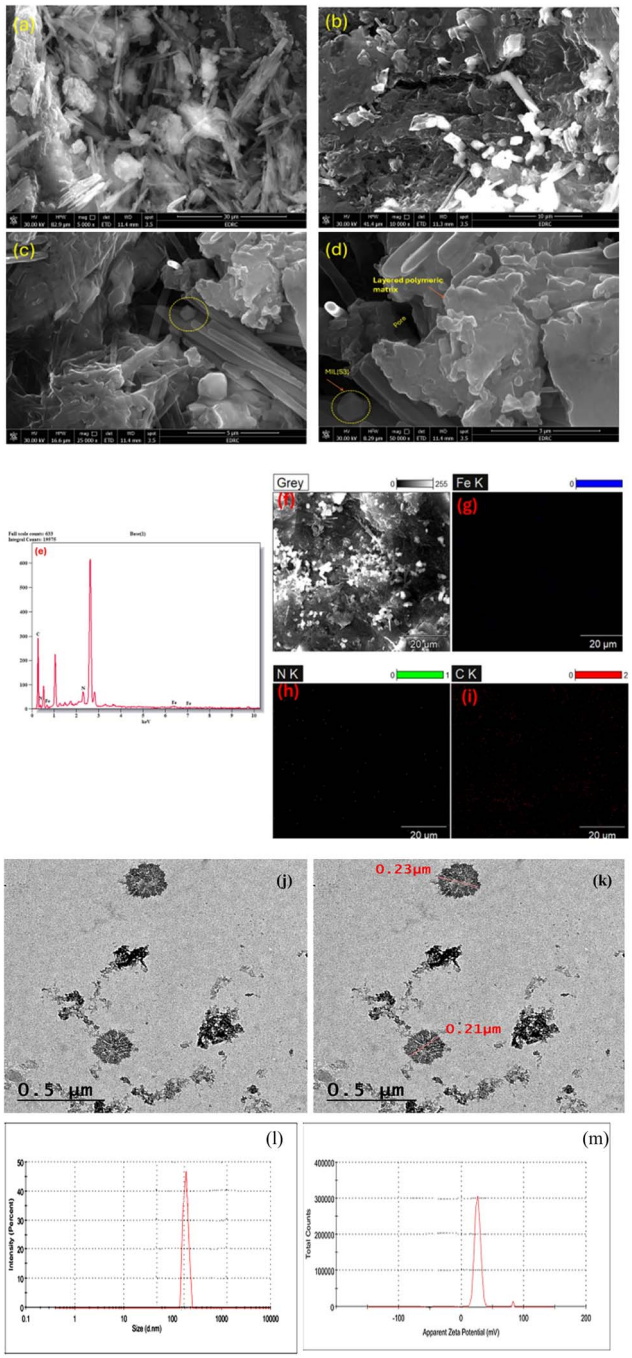

Fig. 8 FE-SEM micrographs of the Ch/MOF composite: (a and b) morphology at different magnifications showing MOF crystals within the chitosan matrix. (c and d) Morphology of the drug-loaded composite (Ch/MOF/Lys/Gent/CIP). (e–i) Corresponding EDX elemental mapping showing the distribution of C, N, and Fe; (j and k) TEM images of the drug-loaded composite (Ch/MOF/Lys/Gent/CIP) showing spherical nanoparticles with measured core diameters of approximately 210 nm and 230 nm (indicated by arrows). (l) Particle size distribution and (m) zeta potential measurements of the optimized Ch/MOF/Lys/Gent/CIP nanoparticles.

Interestingly, the nanocarrier components themselves also showed notable, though moderate, binding potential. D-Glucosamine, representing the chitosan polymer, and terephthalic acid, the organic linker of MIL-53(Fe), docked with scores of −4.31 and −4.01 kcal mol^{-1}, respectively (Fig. 9D and E). This finding implies that the carrier is not a pharmacologically inert vehicle. The cationic chitosan and the MOF framework, upon degradation or sustained interaction at the infection site, could release moieties (glucosamine oligomers, terephthalate) that may act as auxiliary anti-virulence agents, potentially perturbing the assembly or function of the T3SS.

These computational insights significantly strengthen the mechanistic hypothesis of our hybrid nanoformulation. The exceptional antibacterial synergy observed (Section 3.6) may thus be attributed to a concerted four-pronged attack: (1) the sustained, co-localized release of gentamicin and ciprofloxacin, which not only inhibit essential bacterial processes but may also directly disrupt the cell invasion machinery by binding SipD; (2) the immediate membrane-disrupting action of cationic chitosan and released Fe^{3+} ions, compromising the outer membrane permeability barrier; (3) the enzymatic degradation of the exposed peptidoglycan layer by lysozyme; and (4) the potential auxiliary interference with virulence factor assembly by the carrier degradation products. This multi-mechanistic strategy, combining bactericidal and potential anti-virulence actions, creates a formidable challenge for MDR *Salmonella*, overwhelming both its defensive (resistance genes) and offensive (virulence factors) capabilities. It provides a compelling molecular rationale for why the nanoformulation remains effective against isolates harboring **aadA*-2* and *qnrA* resistance genes and offers a sophisticated approach to reduce the likelihood of future resistance development by applying simultaneous, multi-target pressure.

3.5. Sustained release profile and kinetic analysis

The *in vitro* release study provides definitive evidence of the fundamental advantage conferred by nanoencapsulation: the transformation of rapidly diffusing drug molecules into a controlled, sustained-release delivery system. The free drug combination exhibited a classic burst release profile, characterized by the unhindered diffusion of >85% of all agents through the dialysis membrane within the first 2 hours. In stark and direct contrast, the optimized chitosan-MIL-53(Fe) nanoformulation demonstrated a biphasic and prolonged release over the entire 72-hour study period. A moderated initial release (~25% within 6 hours) was followed by a sustained, near-linear phase, culminating in final cumulative releases of 69.2 ± 3.1% for gentamicin, 59.8 ± 2.8% for ciprofloxacin, and 48.5 ± 2.5% for lysozyme (Fig. 10A–C). This dramatic divergence underscores the nano-carrier's role as a functional rate-controlling matrix.[41,66]

Kinetic modeling was employed to quantify these observed differences and elucidate the underlying release mechanisms (Table 4). For the free drugs, release was best described by the Korsmeyer–Peppas model, with release exponents (n) approaching 1.0, indicating a rapid, relaxation-controlled process typical of an unimpeded solution. Conversely, the release from the nanoformulation for all three agents was most accurately modeled by the Higuchi model (R^2 > 0.98),

Table 3 Docking analysis of nanoformulation components against SipD (*Salmonella typhimurium*, PDB: 2YM9)

Compound/representation	Docking score (kcal mol^{-1})	Key interacting amino acid residues
Florfenicol (reference)	−4.51	Lys182, Lys188, Lys276
Ciprofloxacin	−4.96	Glu237, Lys182, Lys188, Lys276
Gentamicin	−5.58	Ser236, Glu237, Gln233, Ser278, Glu281, Lys279
D-Glucosamine (chitosan unit)	−4.31	Lys182, Lys188
Terephthalic acid (MIL-53 linker)	−4.01	Lys188, Lys276

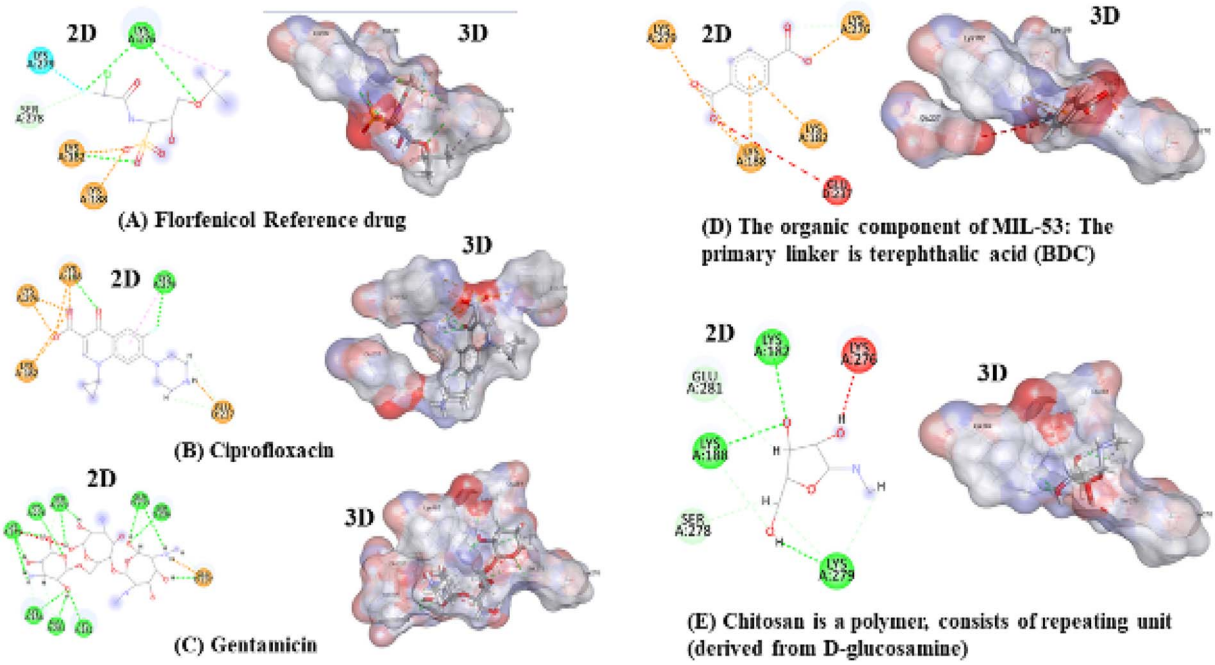

Fig. 9 Molecular docking interactions of 3rd structure selected compounds with SipD from *Salmonella typhimurium* (PDB: 2YM9). (A) Florfenicol (reference drug) showing moderate binding *via* hydrogen-bond and ionic interactions with Lys182, Lys188, and Lys276. (B) Ciprofloxacin exhibiting enhanced stabilization through multiple hydrogen-bond and ionic interactions involving Glu237, Lys182, Lys188, and Lys276. (C) Gentamicin displaying the strongest binding, supported by an extensive hydrogen-bond network with Ser236, Glu237, Gln233, Ser278, Glu281, and Lys279. (D) Terephthalic acid showing weak interactions with Lys188 and Lys276. (E) Chitosan represented by D-glucosamine, forming hydrogen bonds mainly with Lys182 and Lys188.

confirming that the primary release mechanism is Fickian diffusion from within the nanoparticle matrix. A more nuanced analysis using the Korsmeyer–Peppas model revealed agent-specific transport dynamics within the hybrid carrier. The release exponent for encapsulated gentamicin was 0.41, consistent with a process dominated by simple Fickian diffusion. In contrast, the exponents for encapsulated ciprofloxacin (0.58) and lysozyme (0.63) indicate anomalous (non-Fickian) transport, governed by a coupled mechanism of drug diffusion and time-dependent swelling or relaxation of the hydrated chitosan-MOF composite.

The successful control of drug release is clearly shown by the much slower release rates of the nanoencapsulated agents compared to the free drugs (Table 4). This designed release profile offers significant advantages for how the drug behaves in and acts on the body. The quick, all-at-once release of free drugs leads to a pattern of very high drug levels (which can be toxic), followed by a rapid drop to levels that are too low to be effective. This cycle of peaks and troughs is a well-known factor that encourages bacteria to develop resistance. In contrast, the slow, steady release from the nanoformulation is intended to keep drug levels consistently above the level needed to kill bacteria for a long time after just one dose. This explains the stronger antibacterial effect we observed and offers a thoughtful strategy to improve treatment success while reducing the chance that multidrug-resistant *Salmonella* will become even harder to treat. The different ways each drug is released also confirm the smart design of the hybrid nanoparticle system.

3.6. Enhanced and synergistic antibacterial efficacy

The antibacterial activity of individual components and the final optimized Encapsulating Formula (EF) was rigorously evaluated (Fig. 11A–C). Individually, each agent exhibited limited potency against the MDR isolates, which aligns with the moderate to high MIC values (60–500 μg mL^{-1}) reported in

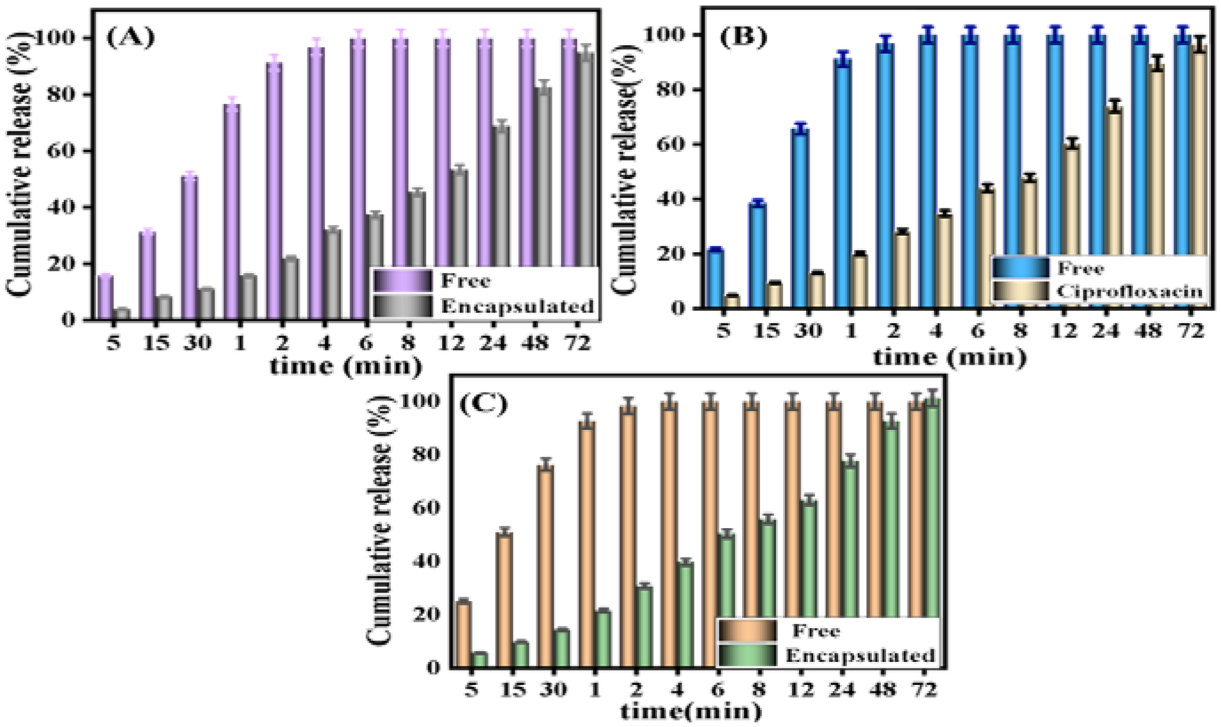

Fig. 10 *In vitro* cumulative release profile (mean ± SD, $n = 3$) of (A) lysozyme, (B) ciprofloxacin, (C) gentamicin from encapsulated (nano-chitocan-MIL-53 MOF composite) and free formulations in phosphate-buffered saline (PBS) medium (0.1 M, pH 7.4) at 37 °C over 72 h.

Table 4 Fitted parameters from kinetic modeling of *in vitro* drug release data

Drug/formulation	Zero-order R^2 (k_0)	First-order R^2 (k_1)	Higuchi R^2 (k_H)	Korsmeyer–Peppas R^2 (k_{KP}, n)
Gentamicin (free)	0.712 (2.81)	0.885 (0.041)	0.823 (15.73)	0.998 (0.92, 0.95)
Gentamicin (encaps.)	0.850 (0.43)	0.902 (0.005)	0.992 (4.12)	0.975 (0.12, 0.41)
Ciprofloxacin (free)	0.698 (2.65)	0.879 (0.038)	0.815 (14.85)	0.999 (0.95, 0.98)
Ciprofloxacin (encaps.)	0.832 (0.31)	0.894 (0.003)	0.985 (3.28)	0.968 (0.09, 0.58)
Lysozyme (free)	0.721 (2.22)	0.862 (0.031)	0.801 (12.41)	0.997 (0.89, 0.90)
Lysozyme (encaps.)	0.818 (0.22)	0.881 (0.002)	0.981 (2.51)	0.962 (0.07, 0.63)

previous studies for chitosan, gentamicin, and ciprofloxacin against various *Salmonella* serovars.[74,75] Reports on the intrinsic activity of MIL-53(Fe) alone are also mixed, with some studies showing minimal effect, and lysozyme is known to have weaker direct activity against Gram-negative bacteria due to the protective outer membrane.[76] In contrast, the integrated EF demonstrated a profound and statistically significant enhancement in potency, transforming these moderately active components into a formidable therapeutic agent.

The EF produced a significantly larger inhibition zone (19.33 ± 1.76 mm) and, most importantly, achieved MIC and MBC values (2.93 and 4.40 μg mL^{-1}, respectively) that were over 25-fold lower than those of the individual antibiotics.

All MBC/MIC ratios were ≤2.5, confirming a potent bactericidal effect. The Fractional Inhibitory Concentration Index (FICI) was calculated to be 0.15, providing irrefutable quantitative evidence of strong synergy (FICI ≤ 0.5).[77]

This exceptional activity stems from a rationally designed, multi-mechanistic, and sequential attack that overcomes the limitations of each component alone. First, the cationic chitosan electrostatically disrupts the negatively charged lipopolysaccharide (LPS) of the outer membrane, altering permeability and causing cell leakage.[78,79] Concurrently, Fe^{3+} ions released from the MIL-53(Fe) framework further destabilize the membrane potential and integrity.[80] This "priming" of the bacterial envelope enables lysozyme to hydrolyze glycosidic bonds in the exposed peptidoglycan layer, thereby inducing cell wall damage and lysis.[81]

The compromised cellular envelope dramatically improves the penetration and intracellular accumulation of the encapsulated antibiotics. This is particularly vital for gentamicin, which alone suffers from poor intracellular penetration that is a key limitation in treating *Salmonella* infections, where the pathogen resides within macrophages.[82] Once inside, gentamicin inhibits protein synthesis by binding the 30S ribosomal subunit, while ciprofloxacin halts DNA replication by targeting DNA gyrase and topoisomerase IV.[83,84] The combination of these two antibiotics is known to be effective in managing systemic

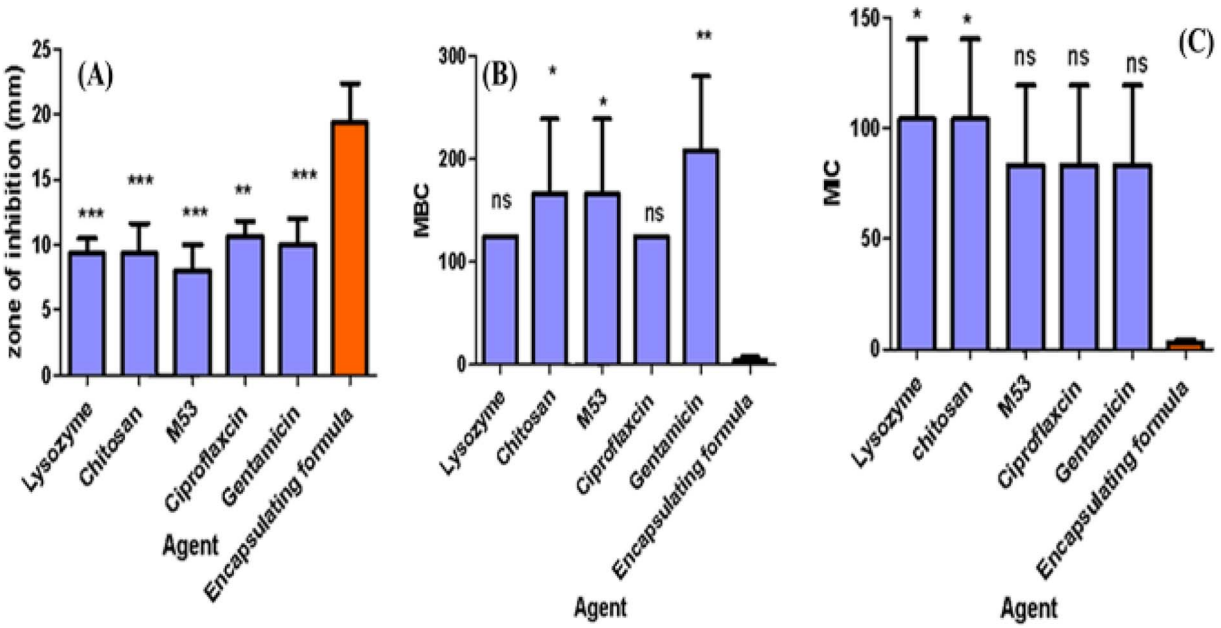

Fig. 11 Encapsulating formula demonstrates superior antibacterial activity through synergistic effects. (A) Zone of inhibition (mm) showing enhanced activity of encapsulating formula (EF, 19.33 ± 1.76 mm) *versus* individual components (8.00–10.67 mm). (B) Minimum bactericidal concentration (MBC, μg mL^{-1}) indicating a marked reduction in the required bactericidal dose for the encapsulating formula (MBC: 4.40 ± 2.20) relative to individual agents (C) minimum inhibitory concentration (MIC, μg mL^{-1}) demonstrating significantly lower inhibitory concentration of the encapsulating formula (MIC: 2.93 ± 0.73) compared to the tested components. Data are presented as mean ± SEM (n = 3). Statistical significance is indicated as *p < 0.05, **p < 0.01, ***p < 0.001, while ns denotes non-significant differences (one-way ANOVA with Tukey's *post hoc* test).

salmonellosis,[85] and here, their co-localization and enhanced delivery potentiate this effect.

This coordinated, multi-target strategy effectively overwhelms bacterial defenses, circumventing the efflux (*qnrA*) and enzymatic inactivation (**aadA*-2*) mechanisms that rendered our isolates phenotypically resistant. The sustained release profile of the EF ensures this synergistic assault is maintained at the infection site, prolonging the therapeutic effect and crucially reducing the potential for resistance development by avoiding prolonged exposure to sub-inhibitory drug concentrations. Thus, the nanoformulation not only restores the efficacy of first-line antibiotics but does so through an intelligent, multi-pronged mechanism that addresses both intrinsic and acquired resistance.

4 Study limitations and future perspectives

4.1. Study limitations

Despite the promising findings, several limitations should be acknowledged. First, the antibacterial efficacy of the developed nanoformulation was demonstrated only under *in vitro* conditions. Although these results provide strong preliminary evidence of its antimicrobial potential, the therapeutic performance of the system under physiological conditions remains to be validated in appropriate *in vivo* infection models.

Second, the present work did not evaluate the potential cytotoxicity of the chitosan-MOF hybrid nanoparticles toward mammalian cells. While Chitosan and MIL-53(Fe) are generally considered biocompatible materials, the biological effects of their combined nanoformulation require careful assessment. Comprehensive toxicological studies including cytotoxicity assays, hemocompatibility evaluation, and histopathological analysis are therefore necessary to confirm the safety profile of the system.

Third, the mechanistic insights regarding anti-virulence activity were primarily derived from computational predictions. Although molecular docking suggested potential interaction with the *Salmonella* SipD protein involved in the Type III secretion system, these findings remain theoretical and require experimental confirmation.

Finally, the long-term physicochemical stability of the optimized nanoparticles under different storage conditions was not systematically investigated. Stability studies are important to determine shelf life and ensure consistent performance during storage and potential practical application.

4.2. Future perspectives

Future research should focus on translating the promising *in vitro* findings into *in vivo* therapeutic validation. Studies using poultry infection models of *Salmonella* should be conducted to evaluate pharmacokinetics, biodistribution, therapeutic efficacy, and safety of the developed nanoformulation.

Further investigations are also needed to validate the proposed anti-virulence mechanism. Experimental studies such as gene expression analysis (*e.g.*, qRT-PCR) of Type III secretion system genes and host-cell invasion assays could confirm

whether the formulation effectively disrupts bacterial virulence pathways.

In addition, comprehensive toxicological profiling should be performed to establish the biocompatibility of the hybrid nanosystem, including cellular toxicity assays and long-term safety evaluations.

From a translational perspective, future work should also address formulation stability, large-scale synthesis, and manufacturing feasibility to facilitate potential veterinary applications. Optimizing scalable production while maintaining the critical quality attributes established through the Quality by Design strategy will be essential for practical implementation.

Overall, addressing these aspects will strengthen the development of this multi-agent nano-delivery platform and support its advancement toward real-world applications for combating multidrug-resistant bacterial infections in veterinary and public health settings.

5 Conclusion

This study successfully addressed a critical dual challenge in veterinary and public health. First, it confirmed the widespread prevalence of multidrug-resistant *Salmonella* in poultry production, with isolates exhibiting resistance to critically important antibiotics like gentamicin and ciprofloxacin, mediated by **aadA*-2* and *qnrA* genes. Second, to combat this threat, a novel and rationally engineered nano-strategy was developed. Using a systematic Quality-by-Design approach, an optimal hybrid nanoformulation was created that synergistically co-encapsulated two antibiotics (gentamicin and ciprofloxacin) and a membrane-disrupting enzyme (lysozyme) within a chitosan-metal–organic framework (MIL-53(Fe)) matrix. The resulting nanoparticles possessed favorable physicochemical properties (248 nm, +33.8 mV) and demonstrated a controlled, sustained release profile over 72 hours, contrasting sharply with the rapid diffusion of free drugs. The nanoformulation exhibited dramatically enhanced *in vitro* antibacterial activity against the MDR *Salmonella* isolates, with MIC values over 25-fold lower than the free drugs. This superior efficacy was driven by strong synergistic interactions among its components (FICI = 0.15), enabling a multi-mechanistic attack that overcame existing resistance mechanisms. Computational docking further supported this multi-target strategy, suggesting potential interference with bacterial virulence through binding to the SipD protein of the Type III secretion system. By combining synergistic antimicrobials with a sustained-release carrier, this work presents a promising advanced delivery platform to enhance therapeutic outcomes in poultry, potentially reduce treatment frequency, mitigate resistance development, and lower the risk of zoonotic transmission.

Conflicts of interest

There are no conflicts of interest to declare.

Data availability

The authors declare that the data supporting the findings of this study are available within the article.

Supplementary information (SI): S1: summary of ANOVA results and model adequacy for the the five quadratic model, as well as S2: physicochemical properties of the optimized chitosan-MIL-53(Fe) nanoformulation. See DOI: https://doi.org/10.1039/d5ra09975g.

Acknowledgements

The authors acknowledge Princess Nourah bint Abdulrahman University Researchers Supporting Project number (PNURSP2026R5), Princess Nourah bint Abdulrahman University, Riyadh, Saudi Arabia.

References

1 K. M. Thomas, W. A. de Glanville, G. C. Barker, J. Benschop, J. J. Buza, S. Cleaveland, M. A. Davis, N. P. French, B. T. Mmbaga and G. Prinsen, Prevalence of *Campylobacter* and *Salmonella* in African food animals and meat: A systematic review and meta-analysis, *Int. J. Food Microbiol.*, 2020, **315**, 108382.

2 E. Rukambile, V. i Sintchenko, G. Muscatello, Q. Wang, J. Kiiru, W. Maulaga, B. Magidanga, G. Banda, R. Kock and R. Alders, *Campylobacter* and *Salmonella* in Scavenging Indigenous Chickens in Rural Central Tanzania: Prevalence, Antimicrobial Resistance, and Genomic Features, *Microbiol. Res.*, 2021, **12**, 440–454.

3 Á. Galán-Relaño, A. Valero Díaz, B. Huerta Lorenzo, L. Gómez-Gascón, M. Á. Mena Rodríguez, E. Carrasco Jiménez, F. Pérez Rodríguez and R. J. Astorga Márquez, *Salmonella* and salmonellosis: An update on public health implications and control strategies, *Animals*, 2023, **13**, 3666.

4 X. Liu, J. Ma, L. Huang, W. Zhu, P. Yuan, R. Wan and K. Hong, Fluoroquinolones increase the risk of serious arrhythmias: a systematic review and meta-analysis, *Medicine*, 2017, **96**, e8273.

5 M. A. S. Khan and S. R. Rahman, Use of phages to treat antimicrobial-resistant Salmonella infections in poultry, *Vet. Sci.*, 2022, **9**, 438.

6 K. Butowska, X. Han, N. Gong, R. El-Mayta, R. M. Haley, L. Xue, W. Zhong, W. Guo, K. Wang and M. J. Mitchell, Doxorubicin-conjugated siRNA lipid nanoparticles for combination cancer therapy, *Acta Pharm. Sin. B*, 2023, **13**, 1429–1437.

7 S. Venkataraman, A. L. Z. Lee, J. P. K. Tan, Y. C. Ng, A. L. Y. Lin, J. Y. K. Yong, G. Yi, Y. Zhang, I. J. Lim and T. T. Phan, Functional cationic derivatives of starch as antimicrobial agents, *Polym. Chem.*, 2019, **10**, 412–423.

8 A. Najafidoust, B. Abdollahi, M. Sarani, M. Darroudi and A. M. Vala, MIL-(53) Fe metal-organic framework (MOF)-based Ag2CrO4 hetrostructure with enhanced solar-light degradation of organic dyes, *Opt. Mater.*, 2022, **125**, 112108.

9 H. Zhang, G. Fu and D. Zhang, Cloning, characterization, and production of a novel lysozyme by different expression hosts, *J. Microbiol. Biotechnol.*, 2014, **24**, 1405–1412.
10 D. Dams and Y. Briers, Enzybiotics: enzyme-based antibacterials as therapeutics, *Ther. Enzym. Funct. Clin. Implic.*, 2019, 233–253.
11 S. W. Ali, M. Joshi and S. Rajendran, Synthesis and characterization of chitosan nanoparticles with enhanced antimicrobial activity, *Int. J. Nanosci.*, 2011, **10**, 979–984.
12 R. K. Farag and R. R. Mohamed, Synthesis and characterization of carboxymethyl chitosan nanogels for swelling studies and antimicrobial activity, *Molecules*, 2012, **18**, 190–203.
13 Y. Lu, W. Geng, L. Li, F. Xie, M. Zhang, H. Xie and J. Cai, Enhanced antibacterial and antibiofilm activities of quaternized ultra-highly deacetylated chitosan against multidrug-resistant bacteria, *Int. J. Biol. Macromol.*, 2025, **298**, 140052.
14 S. Shinde, V. Folliero, A. Chianese, C. Zannella, A. De Filippis, L. Rosati, M. Prisco, A. Falanga, A. Mali and M. Galdiero, Synthesis of chitosan-coated silver nanoparticle bioconjugates and their antimicrobial activity against multidrug-resistant bacteria, *Appl. Sci.*, 2021, **11**, 9340.
15 S. Yu, H. Zhang and C. Li, Solvothermal In-Situ Synthesis of MIL-53(Fe)@Carbon Felt Photocatalytic Membrane for Rhodamine B Degradation, *Int. J. Environ. Res. Publ. Health*, 2023, **20**(5), 4571, DOI: 10.3390/ijerph20054571.
16 D. M. Ávila-Márquez, A. Blanco Flores, H. P. Toledo Jaldin, M. Burke Irazoque, M. González Torres, A. R. Vilchis-Nestor, C. C. Toledo, S. Gutiérrez-Cortez, J. P. Díaz Rodríguez and A. Dorazco-González, MIL-53 MOF on sustainable biomaterial for antimicrobial evaluation against E. coli and S. aureus bacteria by efficient release of Penicillin G, *J. Funct. Biomater.*, 2025, **16**, 295.
17 Z. Liu, H. Deng, Y. Zheng, Y. Tian, Y. Zhang, R. M. Garcia, S. A. Henson Garcia and K. L. Yeung, Synthesis, Characterization, and Toxicity Evaluation of Size-Dependent Iron-Based Metal–Organic Frameworks, *Nanomaterials*, 2025, **15**, 927.
18 İ. Gulcin and S. H. Alwasel, Fe3+ reducing power as the most common assay for understanding the biological functions of antioxidants, *Processes*, 2025, **13**, 1296.
19 X. Qian, B. Yadian, R. Wu, Y. Long, K. Zhou, B. Zhu and Y. Huang, Structure stability of metal-organic framework MIL-53 (Al) in aqueous solutions, *Int. J. Hydrogen Energy*, 2013, **38**, 16710–16715.
20 J. Gordon, H. Kazemian and S. Rohani, MIL-53 (Fe), MIL-101, and SBA-15 porous materials: potential platforms for drug delivery, *Mater. Sci. Eng., C*, 2015, **47**, 172–179.
21 J. Y. Kim, J. W. Suh, J. S. Kang, S. B. Kim, Y. K. Yoon and J. W. Sohn, Gram-negative bacteria's outer membrane vesicles, *Infect. Chemother.*, 2023, **55**, 1.
22 M. Deghelt, S.-H. Cho, J. Sun, S. K. Govers, A. Janssens, A. V. Dachsbeck, H. K. Remaut, K. C. Huang and J.-F. Collet, Peptidoglycan–outer membrane attachment generates periplasmic pressure to prevent lysis in Gram-negative bacteria, *Nat. Microbiol.*, 2025, **10**, 1963–1974.
23 A. Gupta, N. M. Saleh, R. Das, R. F. Landis, A. Bigdeli, K. Motamedchaboki, A. Rosa Campos, K. Pomeroy, M. Mahmoudi and V. M. Rotello, Synergistic antimicrobial therapy using nanoparticles and antibiotics for the treatment of multidrug-resistant bacterial infection, *Nano Futures*, 2017, **1**, 15004.
24 T. Al Hagbani, S. M. D. Rizvi, S. Shakil and A. S. A. Lila, Nano-formulating besifloxacin and employing quercetin as a synergizer to enhance the potency of besifloxacin against pathogenic bacterial strains: a nano-synergistic approach, *Nanomaterials*, 2023, **13**, 2083.
25 W. H. Andrews, H. Wang, A. Jacobson, T. Hammack and F and D Administration, Bacteriological analytical manual (BAM) chapter 5: Salmonella, *Bacteriological Analytical Manual*, 110, 2018, pp. 1–25.
26 M. A. Rahman, T. Ahmad, S. Mahmud, N. C. Barman, M. S. Haque, M. E. Uddin and R. Ahmed, Isolation, identification and antibiotic sensitivity pattern of *Salmonella* spp. from locally isolated egg samples, *Am. J. Pure Appl. Sci.*, 2019, **1**, 1–11.
27 P. A. Wayne, *Clinical and laboratory standards institute: performance standards for antimicrobial susceptibility testing: informational supplement, M100*, Clinical and Laboratory Standards Institute, 2018.
28 S. Singh, A. S. Yadav, S. M. Singh and P. Bharti, Prevalence of *Salmonella* in chicken eggs collected from poultry farms and marketing channels and their antimicrobial resistance, *Food Res. Int.*, 2010, **43**, 2027–2030.
29 R. Govender, I. D. Amoah, A. A. Adegoke, G. Singh, S. Kumari, F. M. Swalaha, F. Bux and T. A. Stenström, Identification, antibiotic resistance, and virulence profiling of *Aeromonas* and *Pseudomonas* species from wastewater and surface water, *Environ. Monit. Assess.*, 2021, **193**, 294.
30 R. A. Walker, E. Lindsay, M. J. Woodward, L. R. Ward and E. J. Threlfall, Variation in clonality and antibiotic-resistance genes among multiresistant *Salmonella enterica* serotype Typhimurium phage-type U302 (MR U302) from humans, animals, and foods, *Microb. Drug Resist.*, 2001, **7**, 13–21.
31 A. Robicsek, J. Strahilevitz, G. A. Jacoby, M. Macielag, D. Abbanat, C. Hye Park, K. Bush and D. C. Hooper, Fluoroquinolone-modifying enzyme: a new adaptation of a common aminoglycoside acetyltransferase, *Nat. Med.*, 2006, **12**, 83–88.
32 N. H. Hoang, T. Le Thanh, R. Sangpueak, J. Treekoon, C. Saengchan, W. Thepbandit, N. K. Papathoti, A. Kamkaew and N. Buensanteai, Chitosan Nanoparticles-Based Ionic Gelation Method: A Promising Candidate for Plant Disease Management, *Polymers*, 2022, **14**(4), 662, DOI: 10.3390/polym14040662.
33 N. Van Bavel, T. Issler, L. Pang, M. Anikovskiy and E. J. Prenner, A Simple Method for Synthesis of Chitosan Nanoparticles with Ionic Gelation and Homogenization, *Molecules*, 2023, **28**, 4328, DOI: 10.3390/molecules28114328.

34 M. Yanat and K. Schroën, Preparation methods and applications of chitosan nanoparticles; with an outlook toward reinforcement of biodegradable packaging, *React. Funct. Polym.*, 2021, **161**, 104849, DOI: 10.1016/j.reactfunctpolym.2021.104849.
35 D. R. Bhumkar and V. B. Pokharkar, Studies on effect of pH on cross-linking of chitosan with sodium tripolyphosphate: A technical note, *AAPS PharmSciTech*, 2006, **7**, 50, DOI: 10.1208/pt070250.
36 S. Özer-önder, Application of Box-Behnken design in the optimization of chitosan nanoparticles prepared by the ionic gelation- ultrasonication method and evaluation of dispersion stability, *J. Res. Pharm.*, 2024, **28**, 1057–1068.
37 R. Scherer, J. Pereira, J. Firme, M. Lemos and M. Lemos, Determination of Ciprofloxacin in Pharmaceutical Formulations Using HPLC Method with UV Detection, *Indian J. Pharm. Sci.*, 2014, **76**(4), 541–544.
38 S. M. Mahgoub, A. M. Radalla, A. A. Allam, H. E. Alfassam and R. Mahmoud, Sustainable RP-HPLC Method for Simultaneous Quantification of Lysozyme and Dequalinium: A Novel Analytical Approach, *J. Pharm. Innovation*, 2025, **20**, 92, DOI: 10.1007/s12247-025-09978-3.
39 S. Loaded, W. Dressing, N. Formulation, A. In and V. Wound, *Egypt. J. Chem.*, 2024, **67**, 445–456, DOI: 10.21608/EJCHEM.2024.252585.8939.
40 J. Chen, D. Cheng, J. Li, Y. Wang, J.-X. Guo, Z.-P. Chen, B.-C. Cai and T. Yang, Influence of lipid composition on the phase transition temperature of liposomes composed of both DPPC and HSPC, *Drug Dev. Ind. Pharm.*, 2012, **39**(2), 197–204, DOI: 10.3109/03639045.2012.668912.
41 A. Ahsan, T. J. Barnes, N. Thomas, S. Subramaniam and C. A. Prestidge, Lipid-based nanocarriers for enhanced gentamicin delivery: a comparative study of liquid crystal nanoparticles and liposomes against Escherichia coli biofilms, *Drug Deliv. Transl. Res.*, 2025, **15**, 4004–4025, DOI: 10.1007/s13346-025-01890-0.
42 P. Costa and J. M. S. Lobo, Modeling and comparison of dissolution profiles, *Eur. J. Pharm. Sci.*, 2001, **13**, 123–133.
43 T. P. Hadjiioannou, G. D. Christian, M. A. Koupparis and P. E. Macheras, *Quantitative Calculations in Pharmaceutical Practice and Research*, VCH, New York, 1993.
44 M. Gibaldi and S. Feldman, Establishment of sink conditions in dissolution rate determinations. Theoretical considerations and application to nondisintegrating dosage forms, *J. Pharm. Sci.*, 1967, **56**, 1238–1242.
45 R. W. Korsmeyer, R. Gurny, E. Doelker, P. Buri and N. A. Peppas, Mechanisms of solute release from porous hydrophilic polymers, *Int. J. Pharm.*, 1983, **15**, 25–35.
46 T. Higuchi, Rate of release of medicaments from ointment bases containing drugs in suspension, *J. Pharm. Sci.*, 1961, **50**, 874–875.
47 M. Balouiri, M. Sadiki and S. K. Ibnsouda, Methods for in vitro evaluating antimicrobial activity: A review, *J. Pharm. Anal.*, 2016, **6**, 71–79.
48 M. P. Weinstein and J. S. Lewis, The clinical and laboratory standards institute subcommittee on Antimicrobial susceptibility testing: Background, organization, functions, and processes, *J. Clin. Microbiol.*, 2020, **58**(3), 01864, DOI: 10.1128/JCM.01864-19.
49 H. Habibi, N. Ghahtan and F. Eskandari, Chemical composition and antibacterial effect of medicinal plants against some food-borne pathogen, *Res. Mol. Med.*, 2017, **5**, 14–21.
50 M. Tyers and G. D. Wright, Drug combinations: a strategy to extend the life of antibiotics in the 21st century, *Nat. Rev. Microbiol.*, 2019, **17**, 141–155.
51 M.O.E. (MOE), *Chemical Computing Group Inc., 1010 Sherbooke St. West, Suite# 910, Montreal, QC, Canada, H3A 2R7*, 2013.
52 S. S. Alkafaas, M. I. Elsalahaty, D. F. Ismail, M. A. Radwan, S. S. Elkafas, S. A. Loutfy, R. M. Elshazli, N. Baazaoui, A. E. Ahmed and W. Hafez, The emerging roles of sphingosine 1-phosphate and SphK1 in cancer resistance: a promising therapeutic target, *Cancer Cell Int.*, 2024, **24**, 89.
53 B. Chea, S. Kong, S. Thim, N. Ban, S. Seng, C. Fernandez-Colorado and K. Kang, Knowledge, attitudes, and practices of antimicrobial use and resistance among livestock producers in Cambodia, *Open J. Anim. Sci.*, 2022, **12**, 454–466.
54 M. E. Basuony, H. A. Aboelmagd and E. K. Bakhiet, Characterization and antimicrobial resistance analysis of *Salmonella enterica* serovar Enteritidis recovered from broiler flocks and fertile eggs in Egypt, *Arch. Agri. Sci. J.*, 2024, **7**, 119–138.
55 M. Abdel-Maksoud, R. Abdel-Khalek, A. El-Gendy, B. L. House, R. F. Gamal and H. M. Abdelhady, Genetic characterisation of multidrug-resistant *Salmonella enterica* serotypes isolated from poultry in Cairo, Egypt, *Afr. J. Lab. Med.*, 2015, **4**, 1–7.
56 N. V Kanu, S. L. Orji, H. A. Okafor, R. I. Adama, F. A. Mustapha, M. P. Oluwafemi, A. B. Offiong, B. C. Tsebam, S. C. Donli and E. O. Ekwe, Molecular Detection of Beta Lactamase Genes from *Salmonella* Typhimurium Isolated from Poultry Droppings in Nyanya, Abuja, *Int. J. Res. Innov. Appl. Sci.*, 2024, **9**, 211–222.
57 M. Muhammad, L. U. Muhammad, A.-G. Ambali, A. U. Mani, S. Azard and L. Barco, Prevalence of *Salmonella* associated with chick mortality at hatching and their susceptibility to antimicrobial agents, *Vet. Microbiol.*, 2010, **140**, 131–135.
58 A. A. Rushdy, F. A. A. Sef, M. I. Mabrouk, Z. H. Kheiralla, S. M. Abd El-All and N. M. Saleh, Use of Different Antibiotic Combinations against Fluoroquinolone-Resistant *Salmonella enterica* from Humans in Egypt, *Egypt. J. Microbiol.*, 2013, **48**, 53–69.
59 T. P. Van Boeckel, C. Brower, M. Gilbert, B. T. Grenfell, S. A. Levin, T. P. Robinson, A. Teillant and R. Laxminarayan, Global trends in antimicrobial use in food animals, *Proc. Natl. Acad. Sci. U. S. A.*, 2015, **112**, 5649–5654.
60 F. A. Khalafalla, S. Basta, E. Hamed and A. H. A. Hassan, Antimicrobial residues in chicken meat, giblet, and skin with referring to maximum residue limits, *J. Adv. Vet. Res.*, 2022, **12**, 234–240.

61 Z. Z. Cao, J. W. Xu, M. Gao, X. S. Li, Y. J. Zhai, K. Yu, M. Wan and X. H. Luan, Prevalence and antimicrobial resistance of *Salmonella* isolates from goose farms in Northeast China, Iran, *J. Vet. Res.*, 2020, **21**, 287.

62 S. P. Dhongade, S. T. Malkapuram, S. H. Sonawane and S. Manickam, High-performance MIL-53 (Fe)-Incorporated Cellulose Acetate Membranes for Efficient Dye and Wastewater Treatment, *Talanta Open*, 2025, 100517.

63 L. Tang, Z. Lv, Y. Xue, L. Xu, W. Qiu, C. Zheng, W. Chen and M. Wu, MIL-53 (Fe) incorporated in the lamellar BiOBr: Promoting the visible-light catalytic capability on the degradation of rhodamine B and carbamazepine, *Chem. Eng. J.*, 2019, **374**, 975–982.

64 X. Wang, Y. Ma, J. Jiang, M. Li, T. Li, C. Li and S. Dong, Cl-based functional group modification MIL-53 (Fe) as efficient photocatalysts for degradation of tetracycline hydrochloride, *J. Hazard. Mater.*, 2022, **434**, 128864.

65 C.-Y. Wang, C.-C. Wang, H.-Y. Chu and P. Wang, Advancing closed-loop plastic economy: Mechanochemical synthesis of MIL-53 (Fe)@ PET (PSM-53) from waste plastics for sustainable antibiotic remediation, *Sci. Total Environ.*, 2025, **1003**, 180730.

66 S. M. Mahgoub, A. S. Alawam, H. A. Rudayni, A. A. Allam, S. A. A. Abdel Aziz, A. A. Eweis, E. Khaled, R. Shafei, F. Mohamed and R. Mahmoud, Lysozyme-dequalinium encapsulation in a Zn-Fe LDH-chia seed matrix for enhanced antimicrobial dental therapeutics, *RSC Adv.*, 2025, **15**, 30872–30899, DOI: 10.1039/d5ra04212g.

67 L. Huang, J. Liu, B. Li, X. Zhao, Z. Cai, X. Wang, Z. Zuo, H. Liu and L. Zhu, Chitosan-copper MOF for corrosion inhibition of Q345 steel: Performance, mechanism, and temperature effects, *Mater. Des.*, 2025, 114227.

68 N. Yang, R. Wang, P. Rao, L. Yan, W. Zhang, J. Wang and F. Chai, The fabrication of calcium alginate beads as a green sorbent for selective recovery of Cu (II) from metal mixtures, *Crystals*, 2019, **9**, 255.

69 Y. Wang, J. Long, W. Xu, H. Luo, J. Liu, Y. Zhang, J. Li and X. Luo, Removal of uranium (VI) from simulated wastewater by a novel porous membrane based on crosslinked chitosan, UiO-66-NH2 and polyvinyl alcohol, *J. Radioanal. Nucl. Chem.*, 2021, **328**, 397–410.

70 F. Ahmadijokani, H. Molavi, A. Bahi, S. Wuttke, M. Kamkar, O. J. Rojas, F. Ko and M. Arjmand, Electrospun nanofibers of chitosan/polyvinyl alcohol/UiO-66/nanodiamond: Versatile adsorbents for wastewater remediation and organic dye removal, *Chem. Eng. J.*, 2023, **457**, 141176.

71 G. Ertürk and B. Mattiasson, Cryogels-versatile tools in bioseparation, *J. Chromatogr. A*, 2014, **1357**, 24–35.

72 H. Zhang, C. Liu, L. Chen and B. Dai, Control of ice crystal growth and its effect on porous structure of chitosan cryogels, *Chem. Eng. Sci.*, 2019, **201**, 50–57.

73 L. N. Tan, N. C. T. Nguyen, A. M. H. Trinh, N. H. N. Do, K. A. Le and P. K. Le, Eco-friendly synthesis of durable aerogel composites from chitosan and pineapple leaf-based cellulose for Cr (VI) removal, *Sep. Purif. Technol.*, 2023, **304**, 122415.

74 A. Shanmugam, K. Kathiresan and L. Nayak, Preparation, characterization and antibacterial activity of chitosan and phosphorylated chitosan from cuttlebone of Sepia kobiensis (Hoyle, 1885), *Biotechnol. Rep.*, 2016, **9**, 25–30.

75 D. H. Shah, X. Zhou, T. Addwebi, M. A. Davis, L. Orfe, D. R. Call, J. Guard and T. E. Besser, Cell invasion of poultry-associated *Salmonella enterica* serovar Enteritidis isolates is associated with pathogenicity, motility and proteins secreted by the type III secretion system, *Microbiology*, 2011, **157**, 1428–1445.

76 C. M. Woods, D. N. Hooper, E. H. Ooi, L.-W. Tan and A. S. Carney, Human lysozyme has fungicidal activity against nasal fungi, *Am. J. Rhinol. Allergy*, 2011, **25**, 236–240.

77 M. Ayaz, A. Sadiq, A. Wadood, M. Junaid, F. Ullah and N. Z. Khan, Cytotoxicity and molecular docking studies on phytosterols isolated from Polygonum hydropiper L, *Steroids*, 2019, **141**, 30–35.

78 M. Kong, X. G. Chen, K. Xing and H. J. Park, Antimicrobial properties of chitosan and mode of action: a state of the art review, *Int. J. Food Microbiol.*, 2010, **144**, 51–63.

79 S.-C. Park, J.-W. Nah and Y. Park, pH-dependent mode of antibacterial actions of low molecular weight water-soluble chitosan (LMWSC) against various pathogens, *Macromol. Res.*, 2011, **19**, 853–860.

80 R. Pachaiappan, S. Rajendran, P. L. Show, K. Manavalan and M. Naushad, Metal/metal oxide nanocomposites for bactericidal effect: A review, *Chemosphere*, 2021, **272**, 128607.

81 A. López-Malo, E. Mani-López, P. M. Davidson and E. Palou, Methods for activity assay and evaluation of results, in *Antimicrob. Food*, CRC Press, 2020, pp. 13–40.

82 S. Mandal, M. D. Mandal and N. K. Pal, Combination effect of ciprofloxacin and gentamicin against clinical isolates of Salmonella enterica serovar Typhi with reduced susceptibility to ciprofloxacin, *Jpn. J. Infect. Dis.*, 2003, **56**, 156–157.

83 S. Ahmed, S. A. Sony, M. B. Chowdhury, M. M. Ullah, S. Paul and T. Hossain, Retention of antibiotic activity against resistant bacteria harbouring aminoglycoside-N-acetyltransferase enzyme by adjuvants: a combination of in-silico and in-vitro study, *Sci. Rep.*, 2020, **10**, 19381, DOI: 10.1038/s41598-020-76355-0.

84 Y. Pommier, E. Leo, H. Zhang and C. Marchand, DNA Topoisomerases and Their Poisoning by Anticancer and Antibacterial Drugs, *Chem. Biol.*, 2010, **17**, 421–433, DOI: 10.1016/j.chembiol.2010.04.012.

85 P. D. Stapleton, S. Shah, J. C. Anderson, Y. Hara, J. M. T. Hamilton-Miller and P. W. Taylor, Modulation of β-lactam resistance in *Staphylococcus aureus* by catechins and gallates, *Int. J. Antimicrob. Agents*, 2004, **23**, 462–467, DOI: 10.1016/j.ijantimicag.2003.09.027.